Bio-based semi-crystalline PEF: Temperature dependence of the constrained amorphous interphase and amorphous chain mobility in relation to crystallization

This is the Author Accepted Manuscript (postprint) version of the following paper: M.C. Righetti, M. Vannini, A. Celli, D. Cangialosi, C. Marega, Bio-based semi-crystalline PEF: Temperature dependence of the constrained amorphous interphase and amorphous chain mobility in relation to crystallization, 2022, peer-reviewed and accepted for publication in Polymer (Polymer 247 (2022) 124771, https://doi.org/10.1016/j.polymer.2022.124771)

Bio-based semi-crystalline PEF: Temperature dependence of the constrained amorphous interphase and amorphous chain mobility in relation to crystallization

Maria Cristina Righetti [1,*], *Micaela Vannini* [2], *Annamaria Celli* [2],

Daniele Cangialosi [3], *Carla Marega* [4]

[1] CNR-IPCF, National Research Council – Institute for Chemical and Physical Processes, Via Moruzzi 1, 56124 Pisa, Italy

[2] Department of Civil, Chemical, Environmental and Materials Engineering, University of Bologna, Via Terracini 28, 40131 Bologna, Italy

[3] Donostia International Physics Center (DIPC), 20018 San Sebastiań, Spain; Centro de Fiśica de Materiales CFM (CSIC-UPV/EHU) and Materials Physics Center MPC, 20018 San Sebastián, Spain

[4] Department of Chemical Sciences, University of Padova, Via Marzolo 1, 35131 Padova, Italy

* corresponding author, email address: cristina.righetti@pi.ipcf.cnr.it

Keywords: Rigid amorphous fraction, Crystallization, Polymorphism, Amorphous chain mobility, Thermodynamic heat capacity, Density

ABSTRACT. The temperature dependence of the constrained amorphous interphase or rigid amorphous fraction (RAF) in bio-based semi-crystalline poly(ethylene 2,5-furandicarboxylate) (PEF) was assessed. RAF, which is located in proximity of the basal crystal planes, was found to develop in parallel with the crystal phase during crystallization at the lowest investigated T_cs, *i.e.* 130 and 140 °C, at which the less stable α'-crystalline phase grows. At higher T_cs, RAF does not vitrify during crystallization, but only upon the subsequent cooling down to T_g. The rigid amorphous fraction at T_g increases by decreasing the crystallization temperature, ranging approximately from 15 to 25%. This information is useful for the development of PEF products, since many RAF physical properties, for example mechanical and barrier properties, are different from those of the amorphous fraction far from the crystals. RAF decreases with increasing temperature, and becomes zero around 150 °C. The same temperature limit of 150 °C was found to influence the reversing crystallization/melting process at the lateral crystal surfaces, as well as the crystallization rate, which reaches its maximum at temperatures above 150 °C. In addition, singularly, the more ordered crystalline α-form was found to grow only at temperatures higher than 150 °C. The total absence of constraints on the amorphous segments mobility, identified at temperatures higher than 150 °C, also favors additional crystallization upon heating in the PEF samples crystallized at low T_cs, with also α-crystals development. The densities of the RAF connected to α'- and α-crystals were estimated at room temperature.

1. INTRODUCTION

In the latest years, furandicarboxylate-based polyesters have been a topic of great interest to both academic and industrial researchers, due to their bio-based aromatic nature and the excellent mechanical and barrier properties [1-34]. In particular, poly(ethylene 2,5-furandicarboxylate) (PEF) has been widely investigated as bio-based substitute of the

petroleum-based counterpart poly(ethylene terephthalate) (PET). The PEF glass transition is about 10 °C higher than that of PET, which is useful for heat resistant packaging, whereas the melting temperature is approximately 40 °C lower than that of PET, which facilitates extrusion and blow molding processes [34]. It is well known that PEF exhibits higher elastic modulus and remarkably better barrier properties with respect to PET [2-4]. These peculiarities of PEF have been associated to higher chain rigidity, which causes suppression of local motions [3,19], and to helical chain conformations of the amorphous segment, stabilized by π- π stacking of the furan rings [19,28].

The crystal structure of PEF was investigated, and polymorphism was identified [10,11,13,20,33]. Depending on the crystallization temperature, a more disordered and a more ordered crystal phases (α' and α respectively) were identified at T_c < 160 °C and T_c > 160 °C, respectively [10,11,26], whereas a different crystal structure (β-form) was observed in samples crystallized from solution [11]. Monoclinic structures were derived for both the α-phase [13] and the less stable α'-phase [20]. Upon stretching, an additional crystalline structure, different from the α'- and α-forms, was identified, and associated to chain organization in extended form [26].

It is known that the synthesis of PEF presents some criticalities, also connected to the side reactions of ethylene glycol, which tend to overbalance the stoichiometric ratios. To limit this drawback, different catalysts have been used for the synthesis of PEF starting from 2,5-furan dicarboxylic acid (FDCA): tetrabutyl titanate (TBT) resulted to be the most effective catalyst in terms of achieved molecular weight [30]. Titanium-based catalysts are also largely used for the PEF synthesis starting from dimethyl-2,5-furan dicarboxylate ester [2,6,7,18]. Ethylene glycol excess is generally utilized, as well as moderately high catalyst amount. The high amount of diol allows to reduce the polymerization times and reach a higher polymerization degree but, at the same time, causes an increment in the content of diethylene glycol

furandicarboxylate (DEGF) units along the polymeric chain, as a consequence of the etherification side reactions [7,18,27,30]. DEGF contents ranging from 0.5 to 5 % have been reported in the literature, depending on the catalyst and synthesis conditions (as catalyst amount, time of its addition, ethylene glycol excess, temperature and time of polymerization, use of FDCA or dimethyl-2,5-furan dicarboxylate ester (DMFD) as starting material) [7,18,27,30]. Thus, many different variables contribute in a non-convergent way to the final amount of DEGF. The problem of the DEGF formation during polymerization, which is seldom considered [7,18,27,30], is actually crucial for the final characteristics of the material: in the case of PET, for instance, it leads to a decrement of melting temperature, glass transition temperature, crystallization rate and degradation resistance [35,36]. Regular chain composition favors crystallization, whereas chemical modification through copolymerization leads often to the rejection of the co-units from the crystal lattice, with the result that the amorphous segments mobility changes far away from the crystals, but also in proximity of the crystals, due to the counits accumulation at the amorphous/crystal boundary [37]. In any case, the overall phase composition is modified by the presence of comonomers.

A complete description of the phase structure of semi-crystalline polymers is a crucial condition for a correct comprehension and prediction of many properties of these materials. In the temperature range between the glass transition temperature (T_g) and the melting temperature (T_m), the solid fraction of most semi-crystalline polymers comprises, besides the crystalline phase, also a constrained or rigid amorphous fraction (RAF), located at the amorphous/crystal boundary close to the lamellae basal planes [38,39]. This constrained amorphous interphase, which arises from irregular and non-adjacent chain folding, is made up of amorphous loops with various length and tie chains connecting different lamellae. The rigid amorphous fraction is characterized by reduced chain mobility with respect to the bulk amorphous phase, because of the connection to the crystalline regions by covalent bonds. By

taking into account this interphase, semi-crystalline polymers belong to the wide class of nanostructured polymeric materials, as nanolayered polymers, nanoconfined polymers, polymeric nanocomposites, block copolymers [40]. All these materials contain nanometric interphases or nanophases with segmental mobility different from the bulk amorphous phase. Presence or absence of covalent bonds, interactions [41] and/or adsorption [42] can lead to a T_g -increase, i.e. a slowing down of segmental dynamics, or T_g -decrease, i.e. acceleration of segmental dynamics.

Recent studies proved that RAF vitrification can occur during crystallization, especially at low temperatures, but also after crystallization, upon cooling to T_g [43-45], due to the reduced chain mobility and stresses not completely released at the crystal surfaces. RAF percentages up to about 20-30 wt% have been calculated for several polymers at T_g [39]. These high values prove how important the RAF quantification is, mainly because many physical properties of the rigid amorphous fraction are different from those of the unconstrained or mobile amorphous fraction (MAF), which vitrifies/devitrifies at T_g [46-55]. This means that the rigid amorphous fraction, if present in high percentage, can influence also macroscopic properties, as for example mechanical and gas permeability properties. As regards the mechanical properties, experimental evidences and theoretical modelling have demonstrated that the elastic modulus of the RAF (E_{RA}) is lower than that of the crystal phase (E_C), but higher than that of the mobile amorphous fraction (E_{MA}), in the order $E_{MA} < E_{RA} < E_C$ [47-49]. Conversely, the density of the RAF (ρ_{RA}) is lower than that of the MAF (ρ_{MA}) [50-52], as the RAF vitrification /devitrification occurs at higher temperatures, where the density is lower [50,53]. This means that the rigid amorphous fraction has an unfavorable influence on the barrier properties, by nullifying the positive effect of the crystalline regions [54,55].

The existence of a rigid amorphous fraction in semi-crystalline PEF samples has been reported in the literature [10,15,17]. The rigid amorphous fraction is commonly calculated at

T_g, and not during the crystallization process, which generally occurs at much higher temperatures. The exact evolution of this PEF nanophase as a function of temperature has never been assessed. Thus, the present study aims precisely to determine how temperature influences the rigid amorphous fraction in PEF. These results will be useful for a better prediction of PEF properties in relation to specific applications.

For this study, a PEF sample prepared with a common catalyst and characterized by a quite low percentage of DEGF units was utilized, to limit, as much as possible, the influence of counits on the evolution and properties of the PEF phase composition.

2. MATERIALS AND METHODS

2.1. Materials

Poly(ethylene furandicarboxylate) (PEF) was prepared according to a synthesis procedure already described in the literature [5,6], but with different times, temperatures and molar ratios, to obtain low DEGF content. Synthesis and purification are reported in the Supplementary Data. Chemical characterization, as described in the Supplementary Data, demonstrated that the weight-average molecular weight (M_w) was 42300, the polydispersity index 2.4, and the molar percentage of DEGF units 2.8%.

2.2. Thermal analysis by Differential Scanning Calorimetry (DSC) and Temperature-Modulated Differential Scanning Calorimetry (TMDSC)

Thermal analysis was performed by means of a Perkin Elmer Calorimeter DSC 8500, equipped with an IntraCooler III as refrigerating system. The instrument was calibrated in temperature with high purity standards (indium, naphthalene, cyclohexane) according to the procedure for standard DSC [56]. Enthalpy calibration was performed with indium. Dry nitrogen was used as purge gas at a rate of 20 mL min^{-1}. To gain precise heat capacity data from the heat flow rate measurements, each scan was accompanied by a blank run with an empty pan. The

sample mass was lower than 10 mg, whereas the mass of the blank and sample aluminum pans matched within 0.02 mg. The temperature of the samples upon heating was corrected for the thermal lag, determined as average by using different standard materials. This lag was 0.05 min, which, for the heating rates of 2, 10, 20 and 40 K min^{-1}, corresponds to a temperature correction of -0.1. -0.5, -1.0 and -2.0 K respectively.

Before each analysis, the PEF samples were heated to 250 °C at 20 K min^{-1} and then maintained at this temperature for 2 min in order to erase the thermal history. Preliminary tests were performed by changing the maximum melting temperature and the residence time (2 min at 250 °C, 5 min at 250 °C and 2 min at 255 °C), and checking the melting behavior after isothermal crystallization at various temperatures: differences were not observed (see Figure S2 of the Supplementary Data).

The thermodynamic solid and liquid specific heat capacities ($c_{p,s}$ and $c_{p,l}$) were measured at 10 K min^{-1} after fast cooling from 250 °C, to obtain totally amorphous PEF samples. However, a rate of -10 K min^{-1} was found sufficient to avoid PEF crystallization upon cooling.

Isothermal crystallizations in the temperature range $130 \leq T_c \leq 190$ °C were performed after quick cooling from 250 °C. The samples were crystallized for times sufficient to obtain the levelling of the heat flow rate signal after the exothermal peak (180 min at 130 °C, 120 min at 140 °C, 90 min at 150 °C, 60 min at 160 and 170 °C, 90 min at 180 °C, and 150 min at 190 °C). The heat evolved during crystallization as a function of time (t) was recorded and the fraction of polymer crystallized after time t ($x_C(t)$) was calculated as the ratio between the heat generated up to time t and the total heat developed during the entire phase transformation ($0 \leq x_C(t) \leq 1$).

The melting behavior subsequent to complete isothermal crystallization in the temperature range $130 \leq T_c \leq 190$ °C was investigated by heating the PEF samples at 10 K min^{-1} directly from T_c and after fast cooling to 20 °C, to obtain apparent specific heat capacity ($c_{p,app}$) curves.

Perfect overlapping of the $c_{p,app}$ curves recorded from T_c and after cooling was observed in the melting temperature range. The melting behavior after crystallization at T_c = 130, 140, 150 and 180 °C was investigated also at different heating rates (2, 20 and 40 K min^{-1}) from the corresponding T_cs.

The amorphous and the semi-crystalline samples crystallized at 130 ≤ T_c ≤ 190 °C were also analyzed, after fast cooling, from 20 °C by TMDSC, with a saw-tooth modulation temperature program, at the average heating rate of 2 K min^{-1}, temperature amplitude (A_T) of 1.0 K and modulation periods (p) of 60, 96, and 120 s, to obtain average specific heat capacity ($c_{p,ave}$) curves and reversing specific heat capacity ($c_{p,rev}$) curves. According to the mathematical treatment of TMDSC data, the modulated heat flow rate curve can be approximated to discrete Fourier series, and separated into average and periodic components [57,58]. The average component is equivalent to the conventional heat flow rate signal under linear temperature program. Thus, the $c_{p,ave}$ curve, calculated from the average heat flow rate at the average heating rate of 2 K min^{-1}, corresponds to $c_{p,app}$ upon linear heating rate of 2 K min^{-1}. Conversely, from the periodic component, the $c_{p,rev}$ curve was obtained, according to the following equation:

$$c_{p,rev}(\omega, T, t) = \frac{A_{HF}(T,t)}{A_T(T,t)} \frac{K(\omega)}{m\omega} \quad (1)$$

where A_{HF} and A_T are the amplitudes of the first harmonic of the modulated heat flow and temperature, respectively, ω is the fundamental frequency of temperature modulation (ω = 2π/p), m the mass of the sample and K(ω) the frequency-dependent calibration factor. The K(ω) value, determined by calibration with sapphire, was 1.06±0.02 for p = 60 s, and 1.00 ± 0.02 for p = 96 and 120 s. Quasi-isothermal crystallizations of PEF were also performed by TMDSC at T_c = 130, 140, 150 and 180 °C, by using a saw-tooth modulation temperature program, with A_T of 1.0 °C and modulation periods of 60, 96 and 120 s.

2.3. X-ray Diffraction (XRD) analysis

XRD analysis were carried out at T_{room} with a Bruker AXS D8 ADVANCE Plus diffractometer (Bruker AXS GmbH, Karlsruhe, Germany) in Bragg-Brentano geometry and Cu-Kα radiation (λ = 0.154 nm). The data were collected using 0.05 °/step and 10 s/step; with 2θ ranging from 5 to 35°. Crystallinity degree was calculated from the ratio between the integrated scattering of the crystalline peaks and the total one (crystalline and amorphous), A_C/A_{TOT}, following the application of the least-squares fit procedure elaborated by Hindeleh and Johnson [59]. Air and incoherent scattering were considered. Topas 6 software (Diffrac.Suite, Bruker) was used for the determination of the crystallinity degree, the peak profile was simulated by a Pearson VII function, a Chebyshev function with two parameters was used for the background. The amorphous profile was calculated starting from the position and shape of the calculated pattern of a totally amorphous sample obtained after fast cooling from the melt, and scaling it appropriately on each pattern of the different PEF samples.

2.4. Density measurements

Density measurements of amorphous and semi-crystalline PEF samples were performed by means of a Micromeritics AccuPyc II 1340 helium pycnometer. The density values, determined at 20°C, were obtained as the average of 10 measurements.

3. RESULTS AND DISCUSSION

3.1. Thermodynamic specific heat capacity of PEF

For an accurate evaluation of the MAF and RAF temperature dependence, the thermodynamic solid and liquid specific heat capacities ($c_{p,s}$ and $c_{p,l}$) of PEF were measured. Figure 1 shows the apparent specific heat capacity ($c_{p,app}$) of initially amorphous PEF measured on heating at 10 K min^{-1}, together with the average specific heat capacity ($c_{p,ave}$) and the reversing specific heat capacity ($c_{p,rev}$) from TMDSC heating scans at different modulation

periods (p = 60, 96 and 120 s) and the average heating rate of 2 K min^{-1}. The thermodynamic solid and liquid specific heat capacities ($c_{p,s}$ and $c_{p,l}$) lines were constructed by extrapolating the $c_{p,app}$, $c_{p,ave}$ and $c_{p,rev}$ data from below the glass transition, and by connecting linearly the melt to the region above T_g, respectively. The derived $c_{p,s}$ and $c_{p,l}$ expressions were: $c_{p,s}$ = 0.99+0.0034·(T-273) and $c_{p,l}$ = 1.58+0.0013·(T-273), with $c_{p,s}$ and $c_{p,l}$ in J g^{-1} K^{-1} and T in K (estimated error: ± 0.02 J g^{-1} K^{-1}).

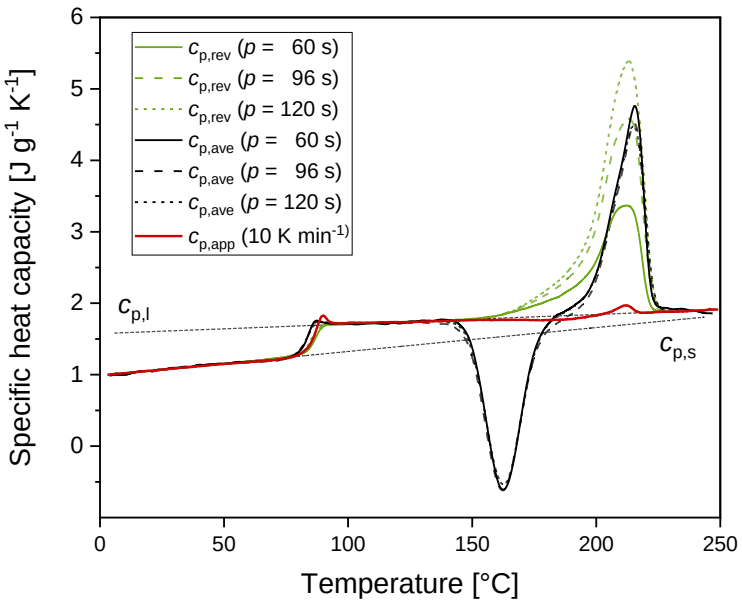

Fig. 1. Apparent specific heat capacity ($c_{p,app}$, red line) at 10 K min^{-1}, average specific heat capacity ($c_{p,ave}$, black lines) and reversing specific heat capacity ($c_{p,rev}$, green lines) at 2 K min^{-1} and various modulation periods (p = 60 s: solid lines, p = 96 s: dashed lines, p = 120 s: dotted lines) of amorphous PEF. The straight black dotted lines are the thermodynamic solid and liquid specific heat capacities ($c_{p,s}$ and $c_{p,l}$).

The glass transition temperature (T_g) is centered at 83 and 85 °C upon heating at 2 and 10 K min^{-1}, respectively, and the corresponding specific heat capacity increment ($\Delta c_{p,a}$) is 0.41 J g^{-1} K^{-1}. The dynamic glass transition, which is observed when the modulation period is equal to the timescale of the cooperative segmental motions, is recognizable from the $c_{p,rev}$ curves at temperatures higher than the corresponding thermal glass transition, which is defined by the $c_{p,ave}$ curves [60].

At temperatures higher than 140 °C, the amorphous PEF undergoes a cold crystallization process, which is more intense at the heating rate of 2 K min^{-1} and barely detectable at 10 K min^{-1}. At 2 K min^{-1} the cold crystallization peak is centered at about 160 °C. The cold crystal growth is accompanied by a reversing melting process, which starts at about 150 °C and extends up to complete fusion. The reversing heat capacity ($c_{p,rev}$) originates from melting/recrystallization processes that can be reversed by temperature modulation. The higher the modulation period, the larger the portions of crystalline regions that melt during the heating semi-periods and recrystallize in the subsequent cooling semi-periods, and, as a consequence, the higher the $c_{p,rev}$ value [38]. The melting peak at 2 K min^{-1} is centered at 215 °C.

3.2. Crystallinity degree of PEF as a function of T_c

Figure 2 collects the $c_{p,app}$ curves after isothermal crystallizations at $130 \leq T_c \leq 190$ °C and fast cooling to below T_g. (The isothermal heat flow signals at the various T_cs are shown in Figure S3 and the corresponding crystallization half-times in Figure S4 of the Supplementary Data, whereas the glass transition region is discussed in a following section.)

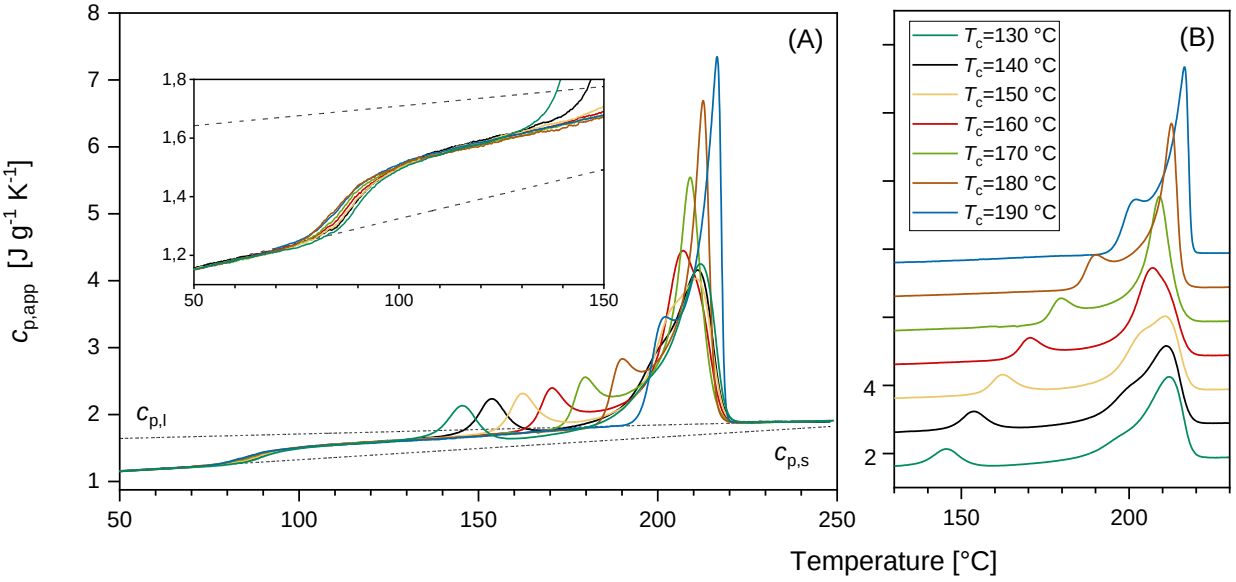

Fig. 2. Apparent specific heat capacity ($c_{p,app}$) curves at 10 K min^{-1} (solid lines) after isothermal crystallization at various T_cs (for the curve colors, see legend in (B)). The black dotted lines are the thermodynamic solid and liquid specific heat capacities ($c_{p,s}$ and $c_{p,l}$). The inset in (A) is an enlargement of the glass transition region. In (B), the $c_{p,app}$ curves in the melting region are shifted vertically for the sake of clearness. The ordinate values in (B) refers only to the bottom curve.

The melting behavior appears dependent on the crystallization temperature. Although it has already been described [10,33], it is here discussed again with the aim of quantifying the crystallinity degree as a function of T_c. Triple and double melting behaviors are exhibited by the PEF samples crystallized at $T_c \leq 160$ °C and $T_c > 160$ °C, respectively [10]. The triple melting behavior was connected with the fusion of the less perfect α'-crystals, which were assumed to grow at $T_c < 160$ °C. The three melting peaks were interpreted as due to fusion, in the order, of (*i*) secondary crystals, (*ii*) original primary crystals and (*iii*) recrystallized crystals [10,33]. Conversely, the double melting behavior for $T_c > 160$ °C was linked to the fusion of the more ordered α-crystals, which develop at higher T_cs [10]. Due to their higher perfection, α-crystals do not undergo recrystallization into a different crystalline population characterized by thicker lamellae, because at high temperature recrystallization rate decreases [61], with the result that the third melting peak disappears, as also reported for the counterpart PET after crystallization at high T_cs [62,63].

Table 1. Crystallization temperature (T_c); glass transition temperature (T_g); melting temperature assumed as the peak temperature of the highest melting peak (T_m) measured at 10 K min^{-1}; enthalpy of melting (Δh_m) measured at 10 K min^{-1}; crystalline weight fraction (w_C^{XRD}) from XRD analysis; enthalpy of melting of 100% crystalline α-crystals at T_m ($\Delta h_m°$); mobile amorphous weight fraction at T_g (w_{MA}); rigid amorphous weight fraction at T_g (w_{RA}) for PEF semi-crystalline samples (estimated errors: ± 0.5 for T_g; ± 0.2 °C for T_m; ± 0.4 J g^{-1} for Δh_m; ± 0.02 for w_C^{XRD}; ± 10 J g^{-1} for $\Delta h_m°$; ± 0.02 for $w_{MA,}$; ± 0.04 for w_{RAF}).

T_c [°C]	T_g [°C]	T_m [°C]	Δh_m [J g^{-1}]	w_C^{XRD}	$\Delta h_m°(T_m)$ [J g^{-1}]	w_{MA} (T_g)	w_{RA} (T_g)
130.0	89.5	211.8	40.9	0.25	-	0.50	0.25
140.0	88.5	211.2	43.4	0.27	-	0.50	0.23
150.0	87.5	210.7	45.0	0.29	-	0.49	0.22
160.0	87.0	207.0	46.4	0.31	-	0.49	0.20
170.0	86.5	209.2	48.0	0.33	145	0.48	0.19
180.0	86.0	212.7	50.4	0.35	144	0.48	0.17
190.0	85.0	216.5	52.8	0.37	143	0.48	0.15

Table 1 lists the measured enthalpy of melting (Δh_m) calculated by applying a linear baseline between the respective T_cs and 225 °C, together with the corresponding peak temperature of the highest melting peak (T_m). The Δh_m plot as a function of T_c (see Figure S5(A) of the Supplementary Data) shows a quite atypical trend, because Δh_m appears proportionally higher after crystallization at $T_c \leq 150$ °C. Also the peak temperature of the highest melting peak shows a discontinuity around $T_c = 150$ °C (see Figure S5(B) of the Supplementary Data).

Table 2. Enthalpy of melting (Δh_m) measured at different heating rates after isothermal crystallization at various T_cs (estimated error for Δh_m: ± 0.4 J g^{-1})

T_c [°C]	Δh_m (2 K min^{-1}) [J g^{-1}]	Δh_m (10 K min^{-1}) [J g^{-1}]	Δh_m (20 K min^{-1}) [J g^{-1}]	Δh_m (40 K min^{-1}) [J g^{-1}]
130.0	45.8	40.9	39.4	39.6
140.0	48.4	43.4	42.3	41.3
150.0	48.2	45.0	44.6	43.7
180.0	49.2	50.4	48.8	48.4

To investigate if additional crystallization can be associated to the reorganization and recrystallization that generally occur upon heating, the melting behavior at different rates (2, 10, 20, 40 K min^{-1}) was investigated after isothermal crystallization at T_c = 130, 140, 150 and 180 °C. Figure S6 of the Supplementary Data shows the resultant $c_{p,app}$ curves, with associated description (nonessential for the present study), whereas Table 2 collects the corresponding Δh_m data. Table 2 shows that the enthalpy of melting of PEF samples crystallized at T_c = 130, 140 and 150 °C increases significantly with reducing the heating rate, which suggests that further crystal growth occurs upon heating simultaneously to reorganization and recrystallization, although also crystal form transformation into the most stable α-form cannot be ruled out. It is worth reminding that, if crystallization and melting occur in sequence during

a heating scan, the sum of enthalpy of crystallization plus enthalpy of melting is always higher than zero, due to the $\Delta h_m°$ increase with temperature [64]. Conversely, for the sample crystallized at T_c = 180 °C, the measured Δh_m is approximately constant, which proves that the melting of enthalpy, and consequently the crystallinity degree, is heating rate independent.

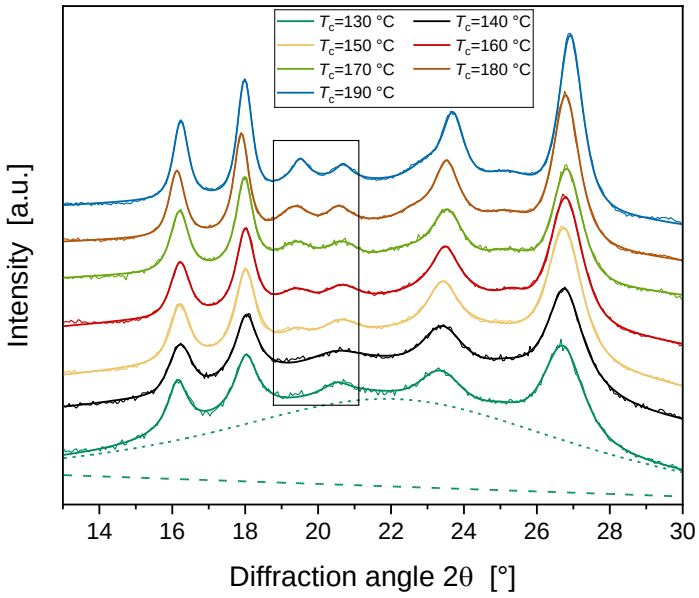

Fig. 3. XRD patterns at T_{room} of PEF samples after isothermal crystallization at the indicated T_cs. The thin curves are the experimental profiles, the thicker curves are the calculated intensities. The patterns have been scaled to obtain similar intensities of the reflection peaks. The black box highlights the main 2θ region that differentiates α'- and α-crystals. For the condition T_c =130 °C, the scattering of the amorphous fraction (short dashed line) is also shown, as well as the background (dashed line).

XRD analysis was performed to identify the crystalline forms that grow at the different T_cs and estimate the crystalline degree. Figure 3 shows the XRD profiles at T_{room} of the PEF samples crystallized at 130 ≤ T_c ≤ 190 °C. In agreement with literature data, the XRD profile of the sample crystallized at T_c = 140 °C, as well as at 130 °C, corresponds to that of the α'-phase, with the typical reflections located at scattering angles 2θ of 16.2, 18.0, 20.5, 23.3 and 26.7 [10,11,20]. Starting from T_c =150 °C, a new reflection emerges at 2θ = 19.4°, with intensity increasing with T_c. This peak has been associated to the α-form [10]. An additional small reflection can be detected at 25.1° for T_c ≥ 160 °C, and, most importantly, a large shoulder

at about 22.5° for $T_c \geq 170$ °C. These measurements suggest that (*i*) α'- crystals grow at $T_c \leq$ 140 °C, (*ii*) α-crystals grow at $T_c \geq 170$ °C, (*iii*) at the intermediate temperatures, $150 \leq T_c \leq$ 160 °C, a mixture of α'- and α-crystals develops, with the α amount increasing with T_c. The crystalline fractions calculated for all the samples from the XRD profiles (w_C^{XRD}) are reported in Table 1. It is worth pointing out that the presence of α-crystals at T_c = 150 °C was not observed in previous studies of PEF samples, for which, unfortunately, the DEGF amount was not quantified [10].

Additional XRD analysis was also carried out (*i*) to verify if the higher Δh_m values measured for the PEF samples crystallized at $T_c \leq 150$ °C has to be ascribed to additional crystallization occurring upon heating, and (*ii*) to investigate if α'- α transformation takes place upon heating. Figure 4 shows the XRD profiles of PEF samples crystallized at T_c =140 °C and heated (*i*) at 2 and 10 K min^{-1} up to 190 °C, (*ii*) at 10 K min^{-1} up to 205 °C and (*iii*) at 2 K min^{-1} up to 210 °C, and then quickly cooled to T_{room}. The patterns of the samples heated up to 190 °C prove that crystal phase does not change upon heating up to this temperature, confirming the presence of only α'-crystals. Instead, crystallinity was found higher than the original one (w_C^{XRD} = 0.34 after heating at 2 and 10 K min^{-1}), which confirms the occurring of additional α'-crystallization for the PEF samples crystallized at low T_cs. Different patterns are exhibited by the samples heated up to 205 and 210 °C. The appearance of the reflection at 19.4° demonstrates that α-crystals develop upon heating at temperatures higher than 190 °C. These extra α-crystals could originate from α'- α transformation, because the crystallinity of the samples heated up to 205 and 210 °C, estimated from the XRD profiles at T_{room}, was found slightly lower than that detected after heating up to 190 °C (w_C^{XRD} = 0.28 after heating at 10 K min^{-1} up to 205 °C and w_C^{XRD} = 0.27 after heating at 2 K min^{-1} up to 210 °C), in agreement with the ongoing melting progress. Some numerical considerations on the correlation between the increased crystallinity upon heating measured by XRD and the Δh_m values determined by

DSC after isothermal crystallizations (see Table 1 and Figure S5(A)) can be found in the Supplementary Data.

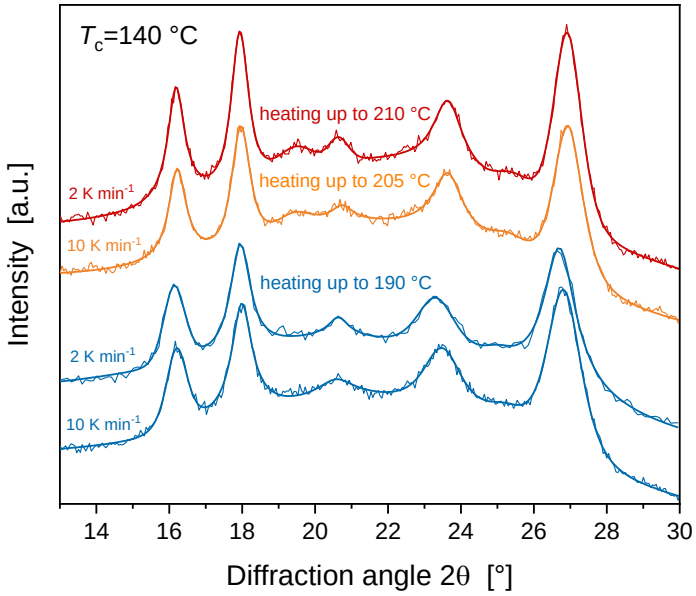

Fig. 4. XRD patterns at T_{room} of PEF samples after isothermal crystallization at T_c = 140 °C and heating at 2 and 10 K min^{-1} up to 190 °C (blue curves), at 10 K min^{-1} up to 205 °C and at 2 K min^{-1} up to 210 °C. The thin curves are the experimental profiles, the thicker curves are the calculated intensities.

Thus, XRD analysis proves that the PEF sample here utilized, after crystallization at low temperature, undergoes further crystallization upon heating, likely also with transformation of α'-crystals into α-crystals. Influence of the catalyst on these events has to be excluded, as the PEF sample was purified. This is a new finding, because additional crystallization and α'-α transformation was not observed in a previous study performed on a PEF sample unfortunately not characterized as regards the DEGF amount [10]. It was reported that PEF crystallization rate increases by reducing the molecular weight and also the DEGF percentage [18], because most likely DEGF counits act as defects for the PEF crystallization process. The crystallization half-times of the PEF sample here utilized are very close (see Figure S4 of the Supplementary Data) to those reported in the previous study [10], although the present molecular weight is almost double. This validates the possibility that the PEF sample of the

previous study was characterized by a higher DEGF amount with respect to the present PEF sample. Thus, high chain regularity and low DEGF percentage could favor extra crystallization at temperatures higher than T_c, and also possible α'-α transformation. However, this feature must be further investigated with more sensitive *in situ* XRD techniques, (*i*) to better clarify the effect of the DEGF counits on the α' and α crystallization ability, (*ii*) to identify distinctly the temperatures at which the additional crystallization and the possible α'-α transformation occur, (*iii*) whether the latter is a solid-solid transition, or proceeds via melting/recrystallization, and (*iv*) to determine confidently the melting temperature of the α-crystals that develop upon heating. As regards this issue, likely the α-crystals melting occurs simultaneously with the melting of the recrystallized α'-crystals, in correspondence of the melting peak at the highest temperature (see Figure 2), because a triple melting behavior is observed both in the presence (this study) and in the absence [10] of α-crystals formation upon heating.

From the w_C^{XRD} values, the enthalpy of melting of 100% crystalline α-crystals was calculated as $\Delta h_m°(T_m) = \Delta h_m(T_m)/ w_C^{XRD}$ for PEF samples crystallized at $T_c \geq 170$ °C (see Table 1). Thus, at the melting temperature, the enthalpy of melting of 100% crystalline α-crystals is approximately 144 J g^{-1}, in excellent agreement with values reported in the literature [6,10]. The $\Delta h_m°$ temperature dependence was also determined according to the general relationship:

$$\Delta h_m°(T) = \Delta h_m°(T_m) + \int_{T_m}^{T} \Delta c_p(T')\, dT' \qquad (2)$$

The derived expression is: $\Delta h_m°(T)$ = 64+0.59·(T-273)-0.001·(T-273)^2 J g^{-1} with T in K (estimated error: ± 10 J g^{-1}). Due to the additional crystallization that occurs upon heating, the enthalpy of melting of 100% crystalline α'-crystals could not be determined by utilizing this procedure.

3.3. Rigid amorphous fraction of PEF as a function of T_c

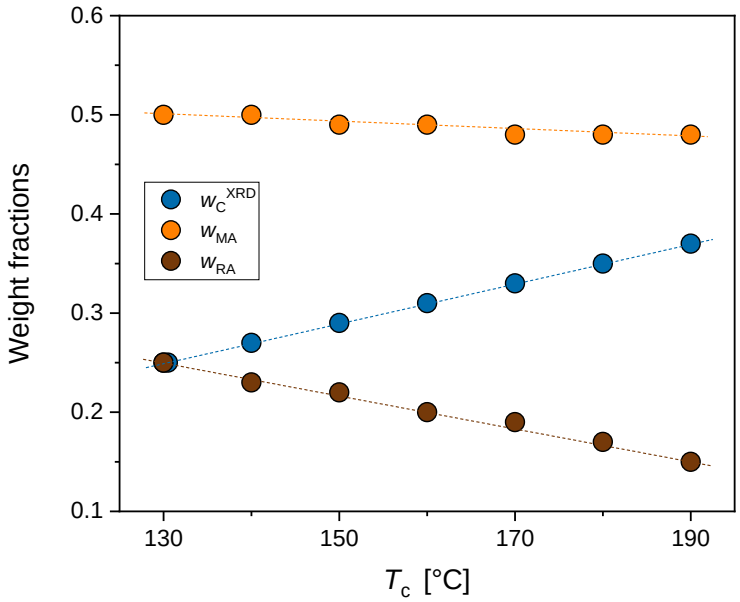

Fig. 5. Crystalline (w_C^{XRD}), mobile amorphous (w_{MA}) and rigid amorphous (w_{RA}) weight fractions of PEF measured at T_g as a function of the crystallization temperature T_c.

For all the PEF samples crystallized in the temperature range $130 \leq T_c \leq 190$ °C, the mobile amorphous fractions (w_{MA}) was determined at the end of the glass transition (see Figure 2), as $w_{MA}=[(c_{p,app} - c_{p,s})/(c_{p,l} - c_{p,s})]$ and the rigid amorphous fraction (w_{RA}) was calculated by difference, being $w_C^{XRD}+ w_{MA}+ w_{RA}=1$. These values are collected in Table 1, together with the T_g values. The trends exhibited by w_C^{XRD}, w_{MA} and w_{RA} as a function of the crystallization temperature are also reported in Figure 5, to better highlight that the phase composition changes monotonically and the transition from the α'-phase T_c-region to the α-phase T_c-region does not involve a composition discontinuity. Figure 5 shows also that the rigid amorphous fraction at T_g increases linearly with decreasing the crystallization temperature and that a higher RAF amount is present at the α'-crystals/amorphous interface.

The enlargement of the T_g region reported in Figure 2 shows that the glass transition shifts to higher temperatures with decreasing the crystallization temperature. This behavior, already observed for other polymers, as for example poly(L-lactic acid) [44], poly(aryl ether ether

ketone) [65] and poly(ethylene-2,6-naphthalenedicarboxylate) [66] can be rationalized as due to progressively increasing restriction and confinement of the MAF regions between the smaller and more dispersed crystals that develop at lower temperatures and likely also to the progressively higher rigid amorphous fraction close to the basal crystal planes.

For various polymers it was proven that rigid amorphous fraction can develop during crystallization, particularly at low temperature, when the chain mobility is low and the formation of regular crystalline structures is more hindered. But RAF can grow also after crystallization, upon cooling to below T_g, due to the progressive lowering in chain mobility and the presence of constraints at the amorphous/crystal interface. Thus, the RAF detected at T_g in the PEF samples crystallized in the range $130 \leq T_c \leq 190$ °C can originate from vitrification occurring during isothermal crystallization and/or upon successive cooling.

To investigate how the crystallization temperature can affect the RAF evolution, quasi-isothermal crystallizations of PEF were performed at different T_cs by TMDSC. This calorimetric technique can allow the simultaneous quantification of the crystalline growth and the evolution of the amorphous fractions during the isothermal crystallization [67].

The $c_{p,rev}$ curves, obtained with different modulation periods (p = 60, 96, and 120 s) during quasi-isothermal crystallization at T_c = 130, 140, 150 and 180 °C, are shown in Figure 6, together with the corresponding evolution of the two-phase baseline specific heat capacity ($c_{p,base,2phase}$), calculated as:

$$c_{p,base,2phase}(t) = w_C^{XRD} x_C(t) c_{p,s} + \left[1 - w_C^{XRD} x_C(t)\right] c_{p,l} \quad (3)$$

where w_C^{XRD} is the final crystal fraction and $x_C(t)$ the fraction of crystallized polymer, obtained by integration of the exothermic heat flow signals.

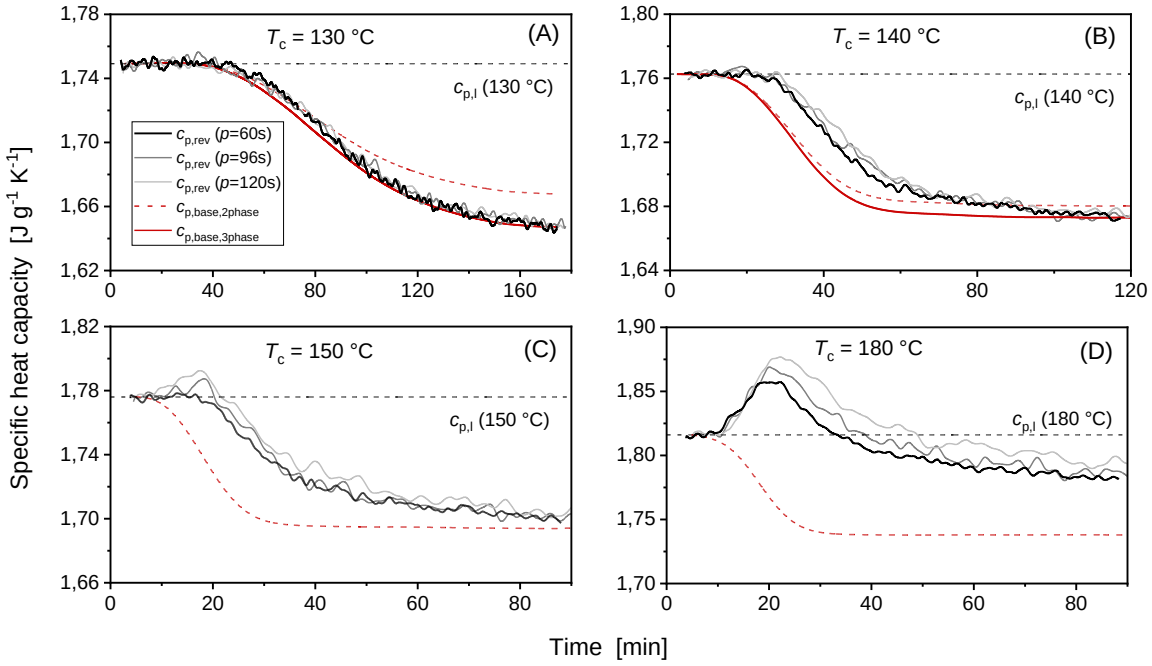

Fig. 6. Time evolution of the reversing specific heat capacity ($c_{p,rev}$) curves of PEF during quasi-isothermal crystallization at the T_cs indicated (130, 140, 150 and 180 °C), together with the calculated baseline specific heat capacities $c_{p,base,2phase}$ and $c_{p,base-3phase}$ (red dashed and solid lines). The black dotted lines are the thermodynamic liquid specific heat capacities ($c_{p,l}$) at the respective T_cs.

For T_c = 130 °C, the three $c_{p,rev}$ curves with different modulation periods overlap within the experimental noise, which means that the reversing heat capacity should correspond to the baseline specific heat capacity of the crystallization process [60]. The reversing heat capacity decays from the liquid specific heat capacity at 130 °C, to a lower value, but the final $c_{p,rev}$ and $c_{p,base,2\text{-}phase}$ values do not coincide. A $c_{p,rev}$ value lower than the final $c_{p,base,2\text{-}phase}$ attests that rigid amorphous fraction develops during crystallization. From the final $c_{p,rev}$ value ($c_{p,rev,final}$), a final RAF amount of 0.07 was estimated as w_{RA}=[($c_{p,l}$ - $c_{p,rev,final}$)/($c_{p,l}$ - $c_{p,s}$)]-w_C^{XRD}. By assuming that, at T_c = 130 °C, the RAF development parallels the crystalline growth, the evolution of a three-phase baseline specific heat capacity ($c_{p,base,3phase}$) was derived as [67]:

$$c_{p,base,3phase}(t) = c_{p,l} - (c_{p,l} - c_{p,rev,final})x_C(t) \quad (4)$$

The good agreement between the $c_{p,rev}$ and the $c_{p,base,3\text{-}phase}$ curves in almost the entire crystallization process, with the exception of a narrow range at intermediate times, confirms

that the reversing heat capacity at T_c = 130 °C substantially represents the baseline heat capacity of the crystallization process.

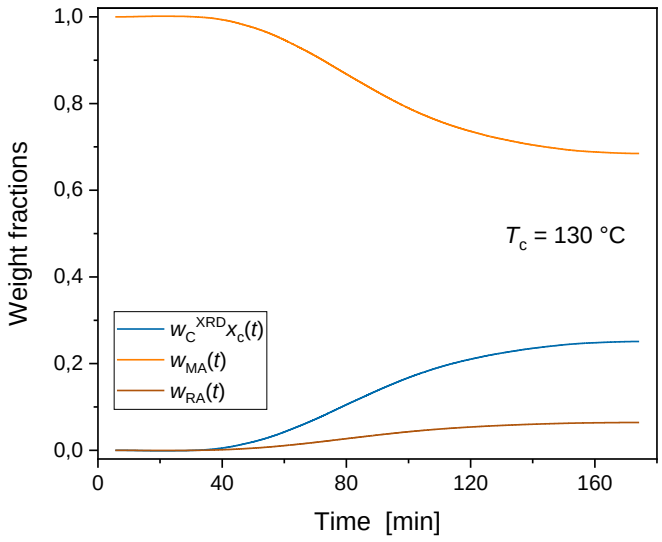

Fig. 7. Evolution of the crystalline ($w_C^{XRD}x_C$), mobile amorphous (w_{MA}) and rigid amorphous (w_{RA}) weight fractions of PEF during crystallization at T_c = 130 °C.

Thus, the evolution of the mobile amorphous (w_{MA}) and rigid amorphous (w_{RA}) fractions during crystallization at T_c = 130 °C was assessed as: $w_{MA}(t)= [c_{p,base,3phase}(t) - c_{p,s}]/(c_{p,l} - c_{p,s})$ and $w_{RA}(t) = 1- w_C^{XRD}x_C(t) - w_{MA}(t)$, respectively. Figure 7 shows that in parallel with the decrease of the mobile amorphous fraction, the crystalline and the rigid amorphous fractions grow simultaneously at T_c = 130 °C, as the RAF is defined as the constrained amorphous fraction at the basal crystal planes. The final w_{RA} is however lower than that detected at T_g (see Table 1), which means that, after crystallization at T_c = 130 °C, further rigid amorphous fraction develops upon cooling to T_g.

Deviation of the $c_{p,rev}$ curve from the baseline heat capacity $c_{p,base,3phase}$ during crystallization is linkable to latent heat exchange occurring during the two modulation semi-periods [38,60]. This excess reversing specific heat capacity ($c_{p,exc} = c_{p,rev} - c_{p,base,3phase}$) identifies a reversing melting process, which is generally dependent on the modulation frequency, because the macromolecule portion that can follow the temperature modulation

(melting in a semi-period and recrystallizing in the successive semi-period) increases with reducing the frequency [68]. For some polymers, as for example polyethylene, poly(butylene succinate) and poly(butylene terephthalate), $c_{p,exc}$ (or $c_{p,rev}$) was found to increase, reach a maximum, and then slowly decrease, especially at high crystallization temperature, where the mobility is high, and during the initial stage of the crystallization, when the process occurs in non-restricted areas [69-71].

Also for the condition T_c = 140 °C (Figure 6B) the difference between the $c_{p,rev}$ curves at different modulation periods is zero at high crystallization times. Due to its modulation period independence, $c_{p,rev,final}$ corresponds to the true final baseline heat capacity. As this value is lower than the final $c_{p,base,2phase}$, also crystallization at T_c = 140 °C involves development of rigid amorphous fraction. A final RAF of approximately 0.03 was calculated for the PEF crystallization at T_c = 140 °C. The excess reversing specific heat capacity is different from zero for almost the entire crystallization time at T_c = 140 °C, attesting the occurrence of reversing melting, i.e. attachment and detachment of chain segments at the lateral surfaces of the crystals during the two modulation semi-periods [38,60].

Figures 6C and 6D show that larger portions of material undergo reversing melting with increasing T_c: $c_{p,rev}$, which appears more dependent on the modulation period, also displays a peak with values higher than the thermodynamic $c_{p,l}$. The reversing heat capacity remains higher than $c_{p,base,2phase}$ for the entire crystallization event. This situation identifies a final condition of continuous fusion and crystallization at the amorphous/crystal interface, as reported for other polymers [38,72]. Due to the presence of intense reversing melting, it is impossible to identify RAF formation during crystallization at T_c =150 and 180 °C. However, it is reasonable to assume that RAF does not develop at these temperatures, because the mobility of the amorphous segments is higher with respect to the condition T_c =140 °C, at which the growth of a very low rigid amorphous fraction (=0.03) was detected.

3.4. Temperature dependence of the rigid amorphous fraction of PEF

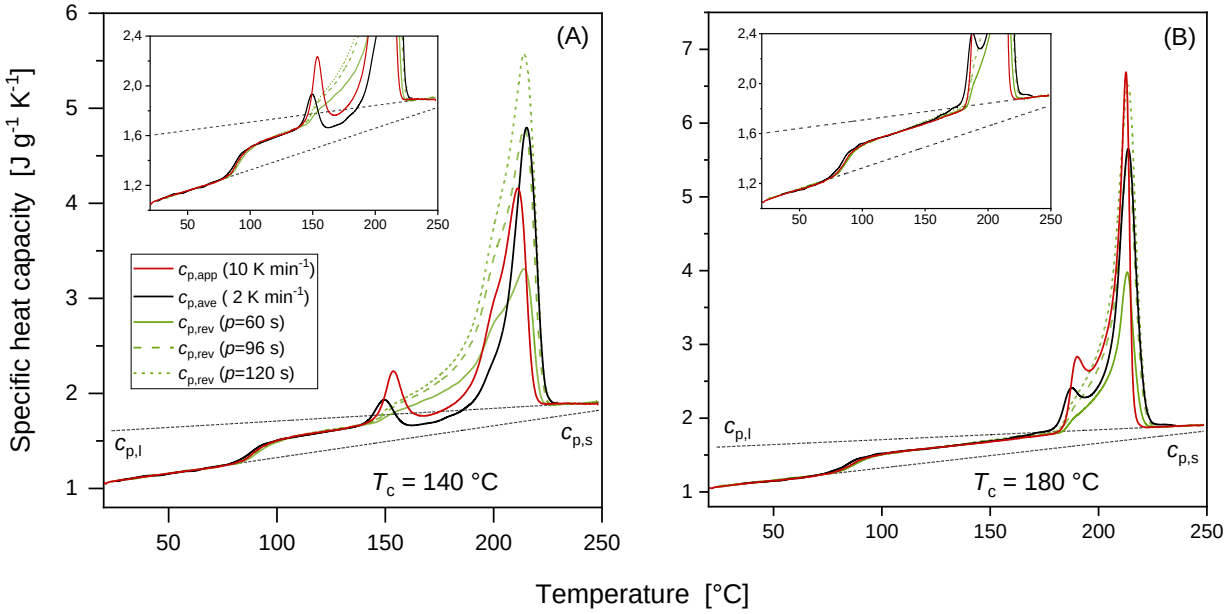

Fig. 8. Specific heat capacities of PEF after crystallization at (A) T_c = 140 °C and (B) T_c = 180 °C as a function of temperature: apparent specific heat capacity ($c_{p,app}$) at 10 K min^{-1}, average specific heat capacity ($c_{p,ave}$) and reversing specific heat capacity ($c_{p,rev}$) at 2 K min^{-1} (p = 60, 96 and 120 s, A_T = 1.0 K). The dotted black lines are the thermodynamic solid and liquid specific heat capacities ($c_{p,s}$ and $c_{p,l}$) of PEF. The insets are enlargements.

Quasi-isothermal crystallizations have demonstrated that not all the RAF detected at T_g develops during crystallization, which necessarily means that rigid amorphous fraction grows partially or totally also upon cooling to T_g. Generally, RAF vitrification upon cooling occurs in a wide temperature range, depending on the distance from the crystals: by increasing the distance from the crystal, the constraints progressively decrease, and vitrification occurs at lower temperatures. It was proven that RAF formation is a true vitrification process, because upon successive heating, devitrification occurs at the same temperature at which the RAF portion had previously vitrified [44].

To quantify the temperature dependence of the rigid amorphous fraction between T_g and T_c, TMDSC measurements were performed after isothermal crystallizations and cooling to below T_g. Figure 8 shows the $c_{p,app}$ curves at 10 K min^{-1}, and the $c_{p,ave}$ and $c_{p,rev}$ curves at 2 K min^{-1} and p = 60, 96 and 120 s, after isothermal crystallization at T_c = 140 and 180 °C. In the

temperature range from T_g to about 135 °C for the sample crystallized at T_c = 140 °C, and to about 150 °C for the samples crystallized at T_c = 180 °C, the $c_{p,app}$, $c_{p,ave}$ and $c_{p,rev}$ curves match within the experimental error. This proves that no reversing latent heat is absorbed or released, and that from T_g up to these temperatures, $c_{p,app}$, $c_{p,ave}$ and $c_{p,rev}$ correspond to the thermodynamic specific heat capacity. At higher temperatures, $c_{p,rev}$ starts to deviate from $c_{p,app}$ and $c_{p,ave}$, attesting the occurrence of reversing melting/recrystallization. Similar behaviors can be observed for the $c_{p,app}$, $c_{p,ave}$ and $c_{p,rev}$ curves after isothermal crystallization at T_c = 130 and 170 °C (see Figure S7 of the Supplementary Data). For these latter crystallization conditions, the $c_{p,app}$, $c_{p,ave}$ and $c_{p,rev}$ curves match from T_g to about 130 °C and 150 °C, respectively.

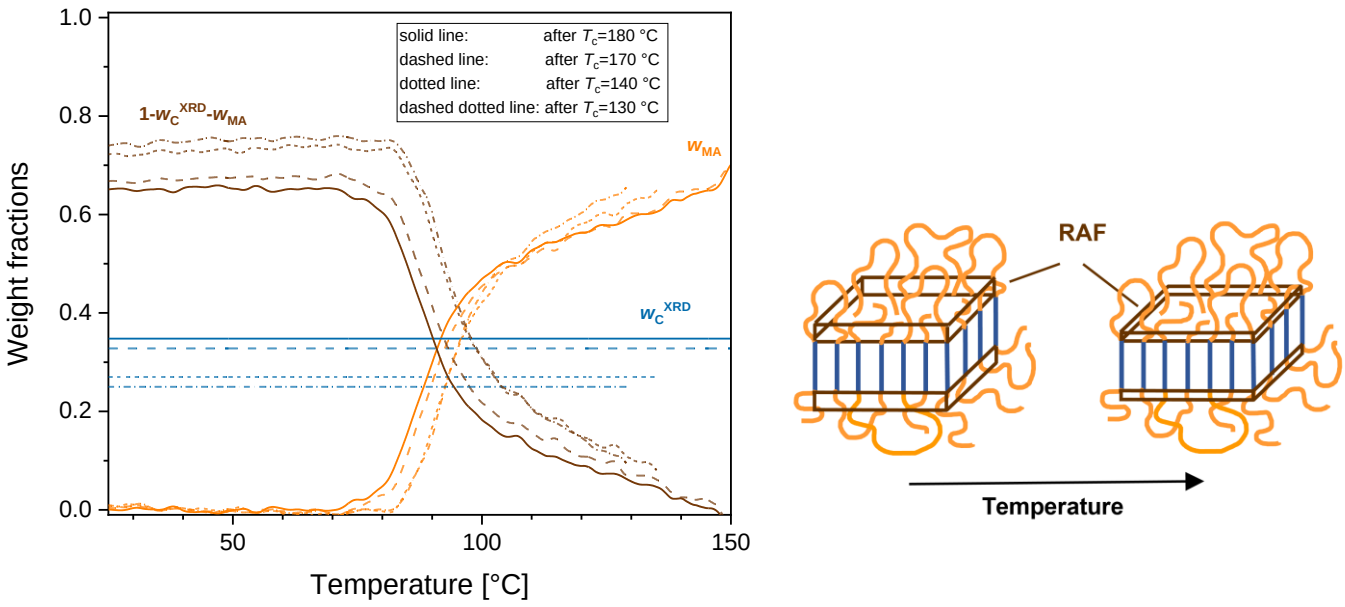

Fig. 9. Temperature dependence of crystalline (w_C^{XRD}), mobile amorphous (w_{MA}) and rigid amorphous (w_{RA}) weight fractions of PEF after isothermal crystallization at the indicated T_cs. On the right, schematic presentation of the RAF temperature dependence above T_g (see text).

From the thermodynamic specific heat capacity, the MAF and RAF temperature dependence were determined as: $w_{MA}(T)$= [$c_{p,rev}(T)$ - $c_{p,s}(T)$]/[$c_{p,l}(T)$ - $c_{p,s}(T)$], and $w_{RA}(T)$ =1-w_C^{XRD} -$w_{MA}(T)$, respectively. Figure 9 shows the temperature dependence of w_{MA} and w_{RA} after crystallization at different T_cs and cooling to below T_g. In the Figure, also the w_C^{XRD} values,

which are constant up to the temperature limit of the $c_{p,app}$, $c_{p,ave}$ and $c_{p,rev}$ curves matching, are displayed. It is worth noting that below T_g, the mobile amorphous fraction is vitrified, so that (1- w_C^{XRD} -w_{MA}) corresponds to the entire amorphous fractions (w_{MA}+w_{RA}).

From Figure 9 it can be deduced that, with increasing temperature, the rigid amorphous fraction decreases from the value at T_g to zero at approximately 150 °C. This finding attests that the limit temperature for the presence of RAF ($T_{g,RAF}$) in PEF samples crystallized at high temperature is about 150 °C, which means that at temperatures higher than 150 °C, the mobility of the amorphous segments close to the basal crystal planes is equal to that of the bulk amorphous phase. It is worth noting that for the samples crystallized at T_c = 130 and 140 °C it is impossible to quantify the RAF limit temperature, as the w_{MA} and w_C^{XRD} evolution above 130 and 135 °C, respectively, cannot be assessed. For these latter crystallization conditions, the RAF amount is approximately 0.09 and 0.06 at 130 and 135 °C respectively, in good agreement with the final RAF values determined at the end of quasi-isothermal crystallizations (see Figure 6).

Thus, the difference ($T_{g,RAF}$ -T_g) for PEF is about 65 K. Similar values have been reported for poly(L-lactic acid), with ($T_{g,RAF}$ -T_g) = 70 K [73,74], for poly(3-hydroxybutyrate), with ($T_{g,RAF}$ -T_g) = 70 K [43], and for poly(1-butene) form II with ($T_{g,RAF}$ -T_g) = 75 K [75,76]. Conversely, higher differences have been estimated for poly(1-butene) form I, with ($T_{g,RAF}$ -T_g) = 125 K [75,76], and for poly(ethylene terephthalate) with ($T_{g,RAF}$ -T_g) = 130 K [77]. Possible explanations of these different behaviors are beyond the scope of this study. Most likely they are connected with the morphology of the crystalline lamellae, with more or less regular chain folding, loops with different length, and possible presence of tie chains. Quite regular chain folding and short loops could be connected to a higher ($T_{g,RAF}$ -T_g) difference. The mobility of long loops is less restricted by the close crystals with respect to short ones, and can be more similar to that of the MAF. Due to its high chain rigidity [15,19], for PEF regular chain re-entry

and short loops could be highly improbable. This supposition can explain the quite low RAF amount detected in PEF, and thus account for the already discussed marked decoupling between the PEF crystalline and the amorphous regions [15].

The complete mobilization of the amorphous segments identified at temperatures higher than 150 °C could trigger the additional crystallization detected upon heating for the PEF samples crystallized at $T_c \leq 150$ °C. The complete mobility of the amorphous segments could favor chain rearrangements and give rise to extra crystal growth at temperatures higher than T_c, also in restricted regions. In addition, it is interesting also to correlate the temperature limit for the presence of RAF with the crystallization rate [10,12] (see also Figure S4 of the Supporting Information). The minimum of the PEF crystallization half-time is located at temperatures slightly above 150 °C, which confirms the dependence of the crystallization rate on the amorphous chain mobility. At temperatures lower than 150 °C, the slower molecular dynamics of the PEF amorphous chains leads to reduced crystallization rates, with also simultaneous development of a small amount of constrained amorphous interphase.

3.5. Density of the rigid amorphous fraction of PEF at T_{room}

The density of amorphous and semi-crystalline PEF samples was measured at 20 °C. The density of the amorphous PEF (ρ_{MA}) was 1.370 ± 0.003 g cm^{-3}, whereas the density of PEF samples crystallized at T_c=140 and 180 °C was 1.389±0.003 and 1.392±0.003 g cm^{-3}, respectively. These data allowed the determination of the density of the rigid amorphous fraction (ρ_{RA}) through the equation:

$$\frac{1}{\rho} = \frac{w_C^{XRD}}{\rho_C} + \frac{w_{MA}}{\rho_{MA}} + \frac{w_{RA}}{\rho_{RA}} \quad (5)$$

where ρ is the experimental density of the semi-crystalline sample and ρ_C the density of the crystal phase. The density of the crystalline α'- and α-phases was assumed equal to 1.567 and 1.549 g cm^{-3}, respectively [13,20]. Thus, the density of the RAF linked to the α'-crystals turned

out to be 1.3±0.2 g cm^{-3}, whereas the density of the RAF linked to the α-crystals 1.2±0.2 g cm^{-3}, with a clear tendency to lower values with respect to ρ_{MA}: the ρ_{RA} values are approximately 5 and 12% lower than the MAF density. Low RAF density values are theoretically justifiable due to the higher vitrification temperature of the RAF, which necessarily implies a higher fractional free volume with respect to the MAF [50]. In addition, the RAF density can depend on the crystalline form, in case of polymorphism. As already observed for poly(L-lactic acid) [49], the density of the RAF connected to the more ordered α-form appears slightly lower than the density of the RAF connected to the more disordered α'-modification. For PEF, the reduction of the RAF densities with respect to the MAF density is in percentage very close to that determined for the two crystal forms of poly(L-lactic acid) [49]. The tighter chain packing of the α-form could produce a stronger coupling at the amorphous/crystal interface, which could delay the relaxation of the closest amorphous segments, with the result that a higher free volume remains trapped in proximity of the crystals.

4. CONCLUSIONS

Structural characterization of semi-crystalline PEF samples characterized by a quite low DEGF content, proved that (*i*) α'- crystals grow at $T_c \leq 140$ °C, (*ii*) α-crystals grow at $T_c \geq 170$ °C, (*iii*) at the intermediate temperatures, $150 \leq T_c \leq 160$ °C, a mixture of α'- and α-crystals develops, with α amount increasing with T_c. After crystallization at $T_c \leq 150$ °C, supplementary crystallization was detected to occur upon heating, with also likely α'- α transformation. This event was explained as due to the complete mobilization of the amorphous segments, identified around 150 °C, as RAF was found zero at temperatures higher than 150 °C. Thus, the total absence of constraints on the amorphous segments mobility was supposed to favor additional

crystallization at temperatures higher than 150 °C in the PEF samples crystallized at low T_cs, in combination with high compositional chain regularity and low DEGF amount.

Singularly, the more ordered α-crystals grows only at temperatures higher than 150 °C, because the conformational rearrangements that precede crystallization (the *gauge-trans* of the ethylene glycol moiety, and the *anti-syn* of the 2.5-furan dicarboxylate group), needed to establish the extended zigzag conformation typical of this crystalline form [19] require a sufficiently high energy, which evidently can be guaranteed only at temperatures higher than 150 °C. It is worth noting that also for poly(L-lactic acid) exclusive growth of the more perfect α-crystals occurs above the temperature limit for the RAF presence, identified around 130 °C [73,74,78].

The same temperature limit of 150 °C was found to influence the reversing melting, *i.e.* attachment and detachment of chain segments at the lateral surfaces of the crystals upon temperature modulation. At temperature higher than 150 °C, the high mobility of the amorphous segments leads to continuous fusion and crystallization, also after completion of crystallization, and therefore in more restricted areas.

The rigid amorphous fraction was found to develop in parallel with the crystal phase only during crystallization at the lowest T_cs investigated (T_c = 130 and 140 °C), in combination with the growth of the less perfect α'-crystals. At higher T_cs, RAF does not vitrify during crystallization, due to the high mobility of the amorphous phase at temperatures higher than 150 °C, but only after completion of crystallization, upon the subsequent cooling to T_g.

The rigid amorphous fraction measured at T_g depends on the crystallization temperature, and monotonically increases with reducing T_c. Thus, the T_g increase observed after crystallization at progressively lower T_cs was explained as due to confinement of the MAF regions between less perfect and more dispersed crystals and progressively higher rigid amorphous fraction.

The density of the RAF connected to the α-crystals turned out to be slightly lower with respect to that linked to the α'-crystals, likely due the stronger chain coupling at the amorphous/crystal interface produced by the more ordered crystalline structure.

In summary, this study focuses on the connection between the amorphous mobility and the PEF polymorphism. The PEF sample here utilized, characterized by high compositional chain regularity, has evidenced peculiarities previously not reported for samples with higher chain irregularity, and, in addition, a higher interconnection between the two crystalline forms, α' and α. The aim is that the present study can lead the way to further investigations on the PEF polymorphism in relation to the composition structure and the chain mobility.

CRediT author statement

Maria Cristina Righetti: Conceptualization; Data curation; Formal analysis; Investigation; Methodology; Supervision; Writing - original draft; Writing - review & editing; Micaela Vannini: Investigation, Methodology, Writing - original draft; Writing - review & editing; Annamaria Celli: Resources, Writing - review & editing; Daniele Cangialosi: Formal analysis, Writing - review & editing; Carla Marega: Formal analysis, Investigation, Methodology, Writing - original draft; Writing - review & editing.

Declaration of interests

The authors declare that they have no known competing financial interests or personal relationships that could have appeared to influence the work reported in this paper.

Acknowledgment

This article is based upon work from COST Action FUR4Sustain, CA18220, supported by COST (European Cooperation in Science and Technology). XRD measurements were performed with a Bruker AXS D8 ADVANCE Plus diffractometer at the PanLab department facility, founded by the

MIUR-"Dipartimenti di Eccellenza" grantNExuS. D.C. acknowledges financial support from the project PGC2018-094548-B-I00 (MICINN-Spain and FEDER-UE) and the project IT-1175-19 (Basque Government).

Supplementary Data

References

[1] A. Gandini, A.J.D. Silvestre, C.P. Neto, A.F. Sousa, M Gomes, The furan counterpart of poly(ethylene terephthalate): An alternative material based on renewable resources, J. Polym. Sci. A Polym. Chem. 47 (2009) 295−298, https://doi.org/10.1002/pola.23130.

[2] R.J.I. Knoop, W. Vogelzang, J. van Haveren, D.S. van Es, High molecular weight poly(ethylene-2,5-furanoate); critical aspects in synthesis and mechanical property determination, J. Polym. Sci. A Polym. Chem. 51 (2013) 4191−4199, https://doi.org/10.1002/pola.26833.

[3] S.K. Burgess, J.E. Leisen, B.E. Kraftschik, C.R. Mubarak, R.M. Kriegel, W.J. Koros, Chain Mobility, Thermal, and Mechanical Properties of Poly(ethylene furanoate) Compared to Poly(ethylene terephthalate), Macromolecules 47 (2014) 1383−1391, https://doi.org/10.1021/ma5000199.

[4] S.K. Burgess, O. Karvan, J.R. Johnson, R.M. Kriegel, W.J. Koros, Oxygen sorption and transport in amorphous poly(ethylene furanoate), Polymer 55 (2014) 4748−4756, https://doi.org/10.1016/j.polymer.2014.07.041.

[5] G.Z. Papageorgiou, V. Tsanaktsis, D.G. Papageorgiou, S. Exarhopoulos, M. Papageorgiou, D.N. Bikiaris, Evaluation of polyesters from renewable resources as alternatives to the current fossil-based polymers. Phase transitions of poly(butylene 2,5-furan-dicarboxylate), Polymer 55 (2014) 3846−3858, https://doi.org/10.1016/j.polymer.2014.06.025.

[6] G.Z. Papageorgiou, V. Tsanaktsis, D.N. Bikiaris, Synthesis of poly(ethylene furandicarboxylate) polyester using monomers derived from renewable resources: thermal behavior comparison with PET and PEN, Phys. Chem. Chem. Phys. 16 (2014) 7946−7958, https://doi.org/10.1039/C4CP00518J.

[7] S. Thiyagarajan, W. Vogelzang, R.J.I. Knoop, A.E. Frissen, J. Van Haveren, D.S. van Es, Biobased furandicarboxylic acids (FDCAs): effects of isomeric substitution on polyester synthesis and properties, Green Chem. 16 (2014) 1957−1966, https://doi.org/10.1039/C3GC42184H.

[8] A. Codou, N. Guigo, J. Van Berkel, E. de Jong, N. Sbirazzuoli. Non-isothermal Crystallization Kinetics of Biobased Poly(ethylene 2,5-furandicarboxylate) Synthesized via the Direct Esterification Process, Macromol. Chem. Phys. 215 (2014) 2065−2074, https://doi.org/10.1002/macp.201400316.

[9] M. Vannini, P. Marchese, A. Celli, C. Lorenzetti, Fully biobased poly(propylene 2,5-furandicarboxylate) for packaging applications: excellent barrier properties as a function of crystallinity, Green Chem. 17 (2015) 4162−4166, https://doi.org/10.1039/C5GC00991J.

[10] G. Stoclet, G. Gobius du Sart, B. Yeniad, S. de Vos, J.M. Lefebvre, Isothermal crystallization and structural characterization of poly(ethylene-2,5-furanoate), Polymer 72 (2015) 165−176, https://doi.org/10.1016/j.polymer.2015.07.014.

[11] V. Tsanaktsis, D.G. Papageorgiou, S. Exarhopoulos, D.N. Bikiaris, G.Z. Papageorgiou, Crystallization and Polymorphism of Poly(ethylene furanoate), Cryst. Growth Des. 15 (2015) 5505−5512, https://doi.org/10.1021/acs.cgd.5b01136.

[12] J.G. van Berkel, N. Guigo, J.J. Kolstad, L. Sipos, B. Wang, M.A. Dam, N. Sbirrazzuoli, Isothermal Crystallization Kinetics of Poly(Ethylene 2,5-Furandicarboxylate), Macromol. Mater. Eng. 300 (2015) 466−474, https://doi.org/10.1002/mame.201400376.

[13] Y. Mao, R.M. Kriegel, D.G. Bucknall, The crystal structure of poly(ethylene furanoate), Polymer 102 (2016) 308−314, https://doi.org/10.1016/j.polymer.2016.08.052.

[14] G.Z. Papageorgiou, D.G. Papageorgiou, Z. Terzopoulou, D.N. Bikiaris, Production of bio-based 2,5-furan dicarboxylate polyesters: Recent progress and critical aspects in their synthesis and thermal properties, Eur. Polym. J. 83 (2016) 202−229, https://doi.org/10.1016/j.eurpolymj.2016.08.004.

[15] A. Codou, M. Moncel, J.G. van Berkel, N. Guigo, N. Sbirrazzuoli, Glass transition dynamics and cooperativity length of poly(ethylene 2,5-furandicarboxylate) compared to poly(ethylene terephthalate), Phys. Chem. Chem. Phys. 18 (2016) 16647−16658, https://doi.org/10.1039/C6CP01227B.

[16] L. Martino, N. Guigo, J.G. van Berkel, J.J. Kolstad, N. Sbirrazzuoli, Nucleation and Self-Nucleation of Bio-Based Poly(ethylene 2,5-furandicarboxylate) Probed by Fast Scanning Calorimetry, Macromol. Mater. Eng. 301 (2016) 586−596, https://doi.org/10.1002/mame.201500418.

[17] T. Dimitriadis, D.N. Bikiaris, G.Z. Papageorgiou, G. Floudas,. Molecular Dynamics of Poly(ethylene-2,5-furanoate) (PEF) as a Function of the Degree of Crystallinity by Dielectric Spectroscopy and Calorimetry, Macromol. Chem. Phys. 18 (2016) 18, 2056−2062, https://doi.org/10.1002/macp.201600278.

[18] J. Wu, H. Xie, L. Wu, B.-G. Li, P. Dubois, DBU-catalyzed biobased poly(ethylene 2,5-furandicarboxylate) polyester with rapid meltcrystallization: synthesis, crystallization kineticsand melting behavior, RSC Advances 6 (2016) 101578, https://doi.org/10.1039/C6RA21135F.

[19] C.F. Araujo, M.M. Nolasco, P.J.A. Ribeiro-Claro, S. Rudić, A.J.D. Silvestre, P.D. Vaz, A.F. Sousa, Inside PEF: Chain Conformation and Dynamics in Crystalline and Amorphous Domainsc, Macromolecules 51 (2018) 3515−3526, https://doi.org/10.1021/acs.macromol.8b00192.

[20] L. Maini, M. Gigli, M. Gazzano, N. Lotti, D.N. Bikiaris, G.Z. Papageorgiou, Structural Investigation of Poly(ethylenefuranoate) Polymorphs, Polymers 10 (2018) 296, https://doi.org/10.3390/polym10030296.

[21] J.-G. Rosenboom, D.K. Hohl, P. Fleckenstein, G. Storti, M. Morbidelli, Bottle-grade polyethylene furanoate from ringopening polymerisation of cyclic oligomers, Nat. Commun 9 (2018) 9, 2701, https://doi.org/10.1038/s41467-018-05147-y.

[22] H. Xie, L. Wu, B.-G. Li, P. Dubois, Modification of Poly(ethylene 2,5-furandicarboxylate) with Biobased 1,5-Pentanediol: Significantly Toughened Copolyesters Retaining High Tensile Strength and O_2 Barrier Property, Biomacromolecules 20 (2019) 353−364, https://doi.org/10.1021/acs.biomac.8b01495.

[23] A. Bourdet, A. Esposito, S. Thiyagarajan, L. Delbreilh, F. Affouard, R.J.I. Knoop, E. Dargent, Molecular Mobility in Amorphous Biobased Poly(ethylene 2,5- furandicarboxylate) and Poly(ethylene 2,4-furandicarboxylate), Macromolecules 51 (2018) 1937−1945, https://doi.org/10.1021/acs.macromol.8b00108.

[24] C. Menager, N. Guigo, L. Martino, N. Sbirazzuoli, H. Visser, S.A.E. Boyer, N. Billon, G. Monge, C. Combeaud, Strain induced crystallization in biobased Poly(ethylene 2,5- furandicarboxylate) (PEF); conditions for appearance and microstructure analysis, Polymer 158 (2018) 158, 364−371, https://doi.org/10.1016/j.polymer.2018.10.054.
[25] J.G. van Berkel, N. Guigo, H.A.Visser, N. Sbirrazzuoli, Chain Structure and Molecular Weight Dependent Mechanics of Poly(ethylene 2,5-furandicarboxylate) Compared to Poly(ethylene terephthalate), Macromolecules 51 (2018) 8539−8549, https://doi.org/10.1021/acs.macromol.8b01831.
[26] G. Stoclet, J.M. Lefebvre, B. Yeniad, G. Gobius du Sart, S. de Vos, On the strain-induced structural evolution of Poly(ethylene-2,5-furanoate) upon uniaxial stretching: An in-situ SAXS-WAXS study, Polymer 134 (2018) 227−241, https://doi.org/10.1016/j.polymer.2017.11.071.
[27] A.S. Joshi, N. Alipourasiabi, Y.-W. Kim, M.R. Coleman, J.G. Lawrence, Role of enhanced solubility in esterification of 2,5-furandicarboxylic acid with ethylene glycol at reduced temperatures: energy efficient synthesis of poly(ethylene 2,5-furandicarboxylate), React. Chem. Eng. 3 (2018) 447−453, https://doi.org/10.1039/C8RE00086G.
[28] G. Papamokos, T. Dimitriadis, D.N. Bikiaris, G.Z. Papageorgiou, G. Floudas, Chain Conformation, Molecular Dynamics, and Thermal Properties of Poly(n-methylene 2,5-furanoates) as a Function of Methylene Unit Sequence Length, Macromolecules 52 (2019) 6533−6546, https://doi.org/10.1021/acs.macromol.9b01320.
[29] N. Poulopoulou, A. Pipertzis, N. Kasmi, D.N. Bikiaris, D.G. Papageorgiou, G. Floudas, G.Z. Papageorgiou, Green polymeric materials: On the dynamic homogeneity and miscibility of furan-based polyester blends, Polymer 174 (2019) 187−199, https://doi.org/10.1016/j.polymer.2019.04.058.
[30] M.B. Banella, J. Bonucci, M. Vannini, P. Marchese, C. Lorenzetti, A. Celli, Insights into the Synthesis of Poly(ethylene 2,5-Furandicarboxylate) from 2,5-Furandicarboxylic Acid: Steps toward Environmental and Food Safety Excellence in Packaging Applications, Ind. Eng. Chem. Res. 58 (2019) 8955−8962, https://doi.org/10.1021/acs.iecr.9b00661.
[31] J. Wang, L. Sun, Z. Shen, J. Zhu, X. Song, X. Liu, Effects of Various 1,3-Propanediols on the Properties of Poly(propylene furandicarboxylate), ACS Sustainable Chem. Eng. 7 (2019) 3282−3291, https://doi.org/10.1021/acssuschemeng.8b05288.
[32] M.C. Righetti, P. Marchese, M. Vannini, A. Celli, C. Lorenzetti, D. Cavallo, C. Ocando, A.J. Müller, R. Androsch, Polymorphism and Multiple Melting Behavior of Bio-Based Poly(propylene 2,5-furandicarboxylate), Biomacromolecules 21 (2020) 2622−2634, https://doi.org/10.1021/acs.biomac.0c00039.
[33] G. Stoclet, A. Arias, B. Yeniad, S. de Vos, Relationships Between Crystalline Structure and the Thermal Behavior of Poly(ethylene 2,5-furandicarboxylate): An In Situ Simultaneous SAXS-WAXS Study, Polym. Eng. Sci. 59 (2019) 1667−1677, https://doi.org/10.1002/pen.25165.
[34] X. Fei, J. Wang, J. Zhu, X. Wang, X. Liu, Biobased Poly(ethylene 2,5-furanoate): No Longer an Alternative, but an Irreplaceable Polyester in the Polymer Industry, ACS Sustainable Chem. Eng. 8 (2020) 8, 8471−8485, https://doi.org/10.1021/acssuschemeng.0c01862.
[35] I. Seganov, J.M. Schultz, S. Fakirov, Effect of diethylene glycol content and annealing temperature on the structure and properties of poly(ethylene terephthalate), J. Appl. Polym. Sci. 32 (1986) 3371−3392, https://doi.org/10.1002/app.1986.070320202.

[36] W.A. MacDonald, New advances in poly(ethylene terephthalate) polymerization and degradation, Polym. Int. 51 (2002) 923−930, https://doi.org/10.1002/pi.917.
[37] M.L. Di Lorenzo, R. Androsch, M.C. Righetti, The irreversible Form II to Form I transformation in random butene-1/ethylene copolymers, Eur. Polym. J. 67 (2015) 264−273, https://doi.org/10.1016/j.eurpolymj.2015.04.002.
[38] B. Wunderlich, Reversible crystallization and the rigid–amorphous phase in semicrystalline macromolecules, Progr. Polym. Sci. 28 (2003) 383–450, https://doi.org/10.1016/S0079-6700(02)00085-0.
[39] M.L. Di Lorenzo, M.C. Righetti, Crystallization-induced formation of rigid amorphous fraction. Polym. Crystal. 1 (2018) e10023, https://doi.org/10.1002/pcr2.10023.
[40] D.S. Simmons, An Emerging Unified View of Dynamic Interphases in Polymers, Macromol. Chem. Phys. 217 (2016) 137−148, https://doi.org/10.1002/macp.201500284.
[41] P. Rittigstein, J.M. Torkelson, Polymer-Nanoparticles Interfacial Interactions in Polymer Nanocomposites: Confinement Effects on the Glass Transition Temperature and Suppression of Physical ageing. J. Polym. Sci. Polym. Phys. 44 (2006) 2935−2943, https://doi.org/10.1002/polb.20925.
[42] N.G. Perez-de-Eulate, M. Sferrazza, D. Cangialosi, S. Napolitano, Irreversible Adsorption Erases the Free Surface Effect on the T_g of Supported Films of Poly(4-*tert*-butylstyrene). ACS Macro Lett. 6 (2017) 354−358, https://doi.org/10.1021/acsmacrolett.7b00129.
[43] M.C. Righetti, E. Tombari, M.L. Di Lorenzo, The Role of the Crystallization Temperature on the Nanophase Structure Evolution of Poly[(R)-3-hydroxybutyrate], J. Phys. Chem. B 117 (2013) 12303−12311, https://doi.org/10.1021/jp4063127.
[44] M.C. Righetti, D. Prevosto, E. Tombari, Time and Temperature Evolution of the Rigid Amorphous Fraction and Differently Constrained Amorphous Fractions in PLLA, Macromol. Chem. Phys. 217 (2016) 2013−2026, https://doi.org/10.1002/macp.201600210.
[45] H. Chen, P. Cebe, Vitrification and Devitrification of Rigid Amorphous Fraction of PET during Quasi-Isothermal Cooling and Heating, Macromolecules 42 (2009) 288−292, https://doi.org/10.1021/ma802104a.
[46] R. Rastogi, W.P. Vellinga, S. Rastogi, C. Schick, H.E.H. Meijer, The three-phase structure and mechanical properties of poly(ethylene terephthalate). J. Polym. Sci. Polym. Phys. 42 (2004) 2092−210, https://doi.org/10.1002/polb.20096.
[47] P.J. in 't Veld, M. Hütter, G.C. Rutledge, Temperature-Dependent Thermal and Elastic Properties of the Interlamellar Phase of Semicrystalline Polyethylene by Molecular Simulation. Macromolecules 39 (2006) 439−447, https://doi.org/10.1021/ma0518961.
[48] M.C. Righetti, L. Aliotta, N. Mallegni, M. Gazzano, E. Passaglia, P. Cinelli, A. Lazzeri, Constrained Amorphous Interphase and Mechanical Properties of Poly(3-Hydroxybutyrate-co-3- Hydroxyvalerate), Front. Chem. 7 (2019) 790, https://doi.org/10.3389/fchem.2019.00790.
[49] L. Aliotta, M. Gazzano, A. Lazzeri, M.C. Righetti, Constrained Amorphous Interphase in Poly(L-lactic acid): Estimation of the Tensile Elastic Modulus, ACS Omega 5 (2020) 20890−20902, ttps://doi.org/10.1021/acsomega.0c02330.
[50] J. Lin, S. Shenogin, S. Nazarenko, Oxygen solubility and specific volume of rigid amorphous fraction in semicrystalline poly(ethylene terephthalate), Polymer 43 (2002) 4733−4743, https://doi.org/10.1016/S0032-3861(02)00278-1.

[51] B.G. Olson, J. Lin, S. Nazarenko, A.M. Jamieson, Positron Annihilation Lifetime Spectroscopy of Poly(ethylene terephthalate): Contributions from Rigid and Mobile Amorphous Fractions, Macromolecules 36 (2003) 7618−7623, https://doi.org/10.1021/ma034813u.

[52] J. del Rio, A. Etxeberria, N. Lopez-Rodriguez, E. Lizundia, J.R. Sarasua, A PALS Contribution to the Supramolecular Structure of Poly(L-lactide), Macromolecules 43 (2010) 4698−4707, https://doi.org/10.1021/ma902247y.

[53] V.B.F. Mathot, Thermal Characterization of States of Matter, in V.B.F. Mathot (Ed.) Calorimetry and Thermal Analysis of Polymers, Hanser, Munich, 1994, pp. 105-167.

[54] M. Drieskens, R. Peeters, J. Mullen, D. Franco, P.J. Lemstra, D.J. Hristova-Bogaerds, Structure versus properties relationship of poly(lactic acid). I. Effect of crystallinity on barrier properties, J. Polym. Sci. Polym. Phys. 47 (2009) 2247−2258, https://doi.org/10.1002/polb.21822.

[55] S. Fernandes Nassar, A. Guinault, N. Delpouve, V. Divry, V. Ducruet, C. Sollogoub, S. Domenek, Multi-scale analysis of the impact of polylactide morphology on gas barrier properties, Polymer 108 (2017) 163−172, https://doi.org/10.1016/j.polymer.2016.11.047.

[56] S.M. Sarge, W. Hemminger, E. Gmelin, G. Höhne, H. Cammenga, W. Eysel, Metrologically Based Procedures for the Temperature, Heat and Heat Flow Rate Calibration of DSC, J. Therm. Anal. 49 (1997) 1125−1134, https://doi.org/10.1007/BF01996802.

[57] A. Wurm, M. Merzlyakov, C. Schick, Reversible Melting Probed by Temperature Modulated Dynamic Mechanical and Calorimetric Measurements, Colloid Polym. Sci. 276 (1998) 289−296, https://doi.org/10.1007/s003960050242.

[58] R. Androsch, I. Moon, S. Kreitmeier, B. Wunderlich, Determination of Heat Capacity with a Sawtooth−Type, Power Compensated Temperature Modulated DSC, Thermochim. Acta 357-358 (2000) 267−278, https://doi.org/10.1016/S0040-6031(00)00397-X.

[59] A.M. Hindele, D.J. Johnson, The resolution of multipeak data in fibre science, J. Phys. D Appl. Phys. 4 (1971) 259–263, https://doi.org/10.1088/0022-3727/4/2/311.

[60] C. Schick, Temperature modulated differential scanning calorimetry (TMDSC) – basics and applications to polymers, in: S.Z.D. Cheng (Ed.) Handbook of Thermal Analysis and Calorimetry, Elsevier Science B.V., Amsterdam, 2002, pp. 713−810.

[61] H.G. Kim, R.E. Robertson, A New Approach for Estimating the Recrystallization Rate and Equilibrium Melting Temperature, J. Polym. Sci. Polym. Phys. 36 (1998) 133−141, https://biblioproxy.cnr.it:2481/10.1002/(SICI)1099-0488(19980115)36:1<133::AID-POLB15>3.0.CO;2-D.

[62] Y. Kong, J.N. Hay, Multiple melting behavior of poly(ethylene terephthalate), Polymer 44 (2003) 623−633, https://doi.org/10.1016/S0032-3861(02)00814-5.

[63] M.C. Righetti, M. Laus, M.L. Di Lorenzo, Rigid amorphous fraction and melting behavior of poly(ethylene terephthalate), Colloid Polym. Sci. 292 (2014) 1365-1374, https://doi.org/10.1007/s00396-014-3198-8.

[64] R. Seguela, Temperature dependence of the melting enthalpy of pol(ethylene terephthalate) and poly(aryl-ether-ether-ketone), Polymer 34 (1993) 1761−1764, https://doi.org/10.1016/0032-3861(93)90338-B.

[65] S.Z.D. Cheng, M.-Y. Cao, B.Wunderlich, Glass transition and melting behavior of poly(oxy-1,4-phenyleneoxy-1,4-phenylenecarbonyl-1,4-phenylene) (PEEK), Macromolecules 19 (1986) 1868−1876, https://doi.org/10.1021/ma00161a015.
[66] S.Z.D. Cheng, B. Wunderlich, Glass transition and melting behavior of poly (ethylene 2, 6-naphthalenedicarboxylate), Macromolecules 21 (1988) 789−797, https://doi.org/10.1021/ma00181a040.
[67] C. Schick, A. Wurm, A. Mohammed, Formation and disappearance of the rigid amorphous fraction in semicrystalline polymers revealed from frequency dependent heat capacity, Thermochim. Acta 396 (2003) 119−132, https://doi.org/10.1016/S0040-6031(02)00526-9.
[68] R. Androsch, B. Wunderlich, A study of the annealing of poly(ethylene-co-octene)s by temperature modulated and standard differential scanning calorimetry, Macromolecules 32 (1999) 7238–7247, https://doi.org/10.1021/ma9905223.
[69] B. Goderis, H. Reynaers, R. Schernberg, V.B.F. Mathot, M.H.J. Koch, Temperature reversible transitions in linear polyethylene studied by TMDSC and time-resolved, temperature-modulated WAXS/SAXS, Macromolecules 34 (2001) 1779–1787, https://doi.org/ 10.1021/ma001759y.
[70] C. Schick, A. Toda, R. Androsch, The Narrow Thickness Distribution of Lamellae of Poly(butylene succinate) Formed at Low Melt Supercooling, Macromolecules 54 (2021) 3366–3376, https://doi.org/10.1021/acs.macromol.1c00388.
[71] A. Toda, Temperature-modulated fast scanning calorimetry of isothermal crystallization of poly(butylene terephthalate), Polymer 228 (2021) 123936, htpps://doi.org/10.1016/j.polymer.2021.123936.
[72] M.C. Righetti, M.L. Di Lorenzo, M. Angiuli, E. Tombari, Structural Reorganization in Poly(butylene terephthalate) during Fusion, Macromolecules 37 (2004) 9027–9033, https://doi.org/10.1021/ma0492667.
[73] M.C. Righetti, E. Tombari, Crystalline, mobile amorphous and rigid amorphous fractions in poly(L-lactic acid) by TMDSC, Thermochim. Acta 522 (2011) 118–127, https://doi.org/10.1016/j.eurpolymj.2008.05.026.
[74] X. Monnier, D. Cavallo, M.C. Righetti, M.L. Di Lorenzo, S. Marina, J. Martin, D. Cangialosi, Physical Aging and Glass Transition of the Rigid Amorphous Fraction in Poly(L-lactic acid), Macromolecules 53 (2020) 8741–8750, https://doi.org/10.1021/acs.macromol.0c01182.
[75] M.L. Di Lorenzo, M.C. Righetti, B. Wunderlich, Influence of Crystal Polymorphism on the Three-Phase Structure and on the Thermal Properties of Isotactic Poly(1-butene), Macromolecules 42 (2009) 9312–9320, https://doi.org/10.1021/ma901882g.
[76] W. Wang, S.E. Fenni, Z. Ma, M.C. Righetti, D. Cangialosi, M.L. Di Lorenzo, D. Cavallo, Glass transition and aging of the rigid amorphous fraction in polymorphic poly(butene-1), Polymer 226 (2021) 123830, https://doi.org/10.1016/j.polymer.2021.123830.
[77] M.C. Righetti, M. Laus, M.L. Di Lorenzo, Temperature dependence of the rigid amorphous fraction in poly(ethylene terephthalate), Eur. Polym. J. 58 (2014) 60–68, https://doi.org/10.1016/j.eurpolymj.2014.06.005.
[78] T. Kawai, N. Rahman, G. Matsuba, K. Nishida, T. Kanaya, M. Nakano, H. Okamoto, J. Kawada, A. Usuki, N. Honma, K. Nakajima, M. Matsuda, M, Crystallization and Melting Behavior of Poly(L-lactic acid), Macromolecules 40 (2007) 9463−9469, https://doi.org/10.1021/ma070082c.

Bio-based semi-crystalline PEF: Temperature dependence of the constrained amorphous interphase and amorphous chain mobility in relation to crystallization

*Maria Cristina Righetti *, Micaela Vannini, Annamaria Celli,*

Daniele Cangialosi, Carla Marega

SUPPLEMENTARY DATA

A. Synthesis, purification and chemical characterization

Materials. Ethylene glycol (EG) and tetrabutyl titanate (TBT) were purchased from Sigma-Aldrich, whereas dimethyl-2,5-furan dicarboxylate ester (DMFD) was provided by Tetrapak. All the reagents were supplied in high purity and therefore used without further purifications.

Synthesis and purification. The PEF sample was prepared by using only 1.7 equivalent of EG and a low amount of TBT because during this study it was observed that TBT tends to favor the dehydration reaction which leads to DEGF formation.

36.83 g (0.200 mol) of DMFD, 21.10 g (0.340 mol) of EG and 0.085 g (2.51 10-4 mol, 325 ppm of Ti) of TBT were charged into a glass reactor, equipped with a stirrer, a temperature programmer, a vacuum controller and a torque meter. The reactor was immersed into a salt bath preheated to 175°C. The first stage was conducted at atmospheric pressure under nitrogen atmosphere and the mixture was allowed to react for 4h under stirring (200 rpm) with continuous removal of methanol. Then, the temperature was increased up to 190°C and kept for 90 min, and later to 230°C for further 90 min. In the second stage the reaction was heated from 230 to 240°C while the pressure was gradually reduced to 0.017 mbar. These conditions were reached within 3h and 30 min, using a linear gradient of temperature and pressure, and maintained for 30 min. Finally, the reaction temperature was further increased till 250°C and stirred for 60 min. To remove the catalyst, the collected polymer was ground and then dissolved in the mixture chloroform/1,1,1,3,3,3-hexafluoro-2-propanol (HFIP) 2/1 (v/v) and later precipitated in methanol, filtered and oven-dried.

Chemical characterizations. The ^{1}H NMR analysis on the PEF polymer was performed at room temperature on samples dissolved in a mixture of deuterated chloroform /deuterated trifluoroacetic acid 80/20 (v/v), using a Varian Mercury 400 spectrometer, with a 400 MHz proton frequency. The recorded spectrum is shown in Figure S1, where the peak attributions of the protons of the repeating unit, the end-groups and the DEGF units, are reported. In

particular, the DEGF amount was calculated as a molar ratio between the normalized peak due to methylene near to ether functionality (protons “d”, 4.05 ppm) and the sum of this peak, the normalized peak of ester methylene of the repeating unit (protons “a”, 4.76 ppm) and the normalized peak of ending methylenes (protons “f”, 4.12 ppm). The diethylene glycol furandicarboxylate (DEGF) unit, calculated as DEGF % = $[I_d/(I_d+I_a+I_f)]\cdot 100$, was 2.8 mol%.

To determine the molecular weight, gel permeation chromatography (GPC) was carried out. The polymer was dissolved in a mixture of $CHCl_3$/HFIP 90/10 (v/v) and filtered through a Teflon syringe filter. Then, the GPC measurement was performed at 30°C on Hewlett Packard Series 1100 liquid chromatography using a PL gel 5 mm Minimixed - C column and a mixture of $CHCl_3$/HFIP 95/5 (v/v) as eluent with a 0.3 mL/min flow; an Ultra-Violet detector was used and a calibration plot was constructed with monodisperse polystyrene standards. The weight-average molecular weight (M_w) was 42300 and the polydispersity index 2.4.

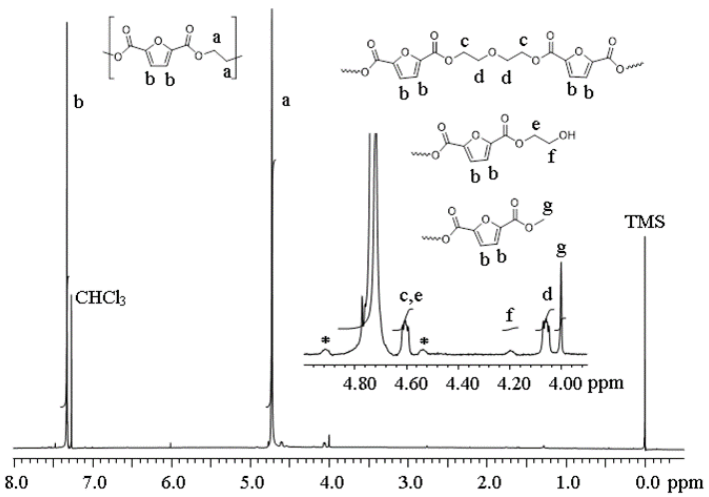

Fig. S1. ^{1}H NMR spectrum of PEF sample, with magnification of the aliphatic region. All the signals are attributed by referring to the letters reported in the chemical structures. The spin side peaks are marked with stars.

B. Thermal analysis

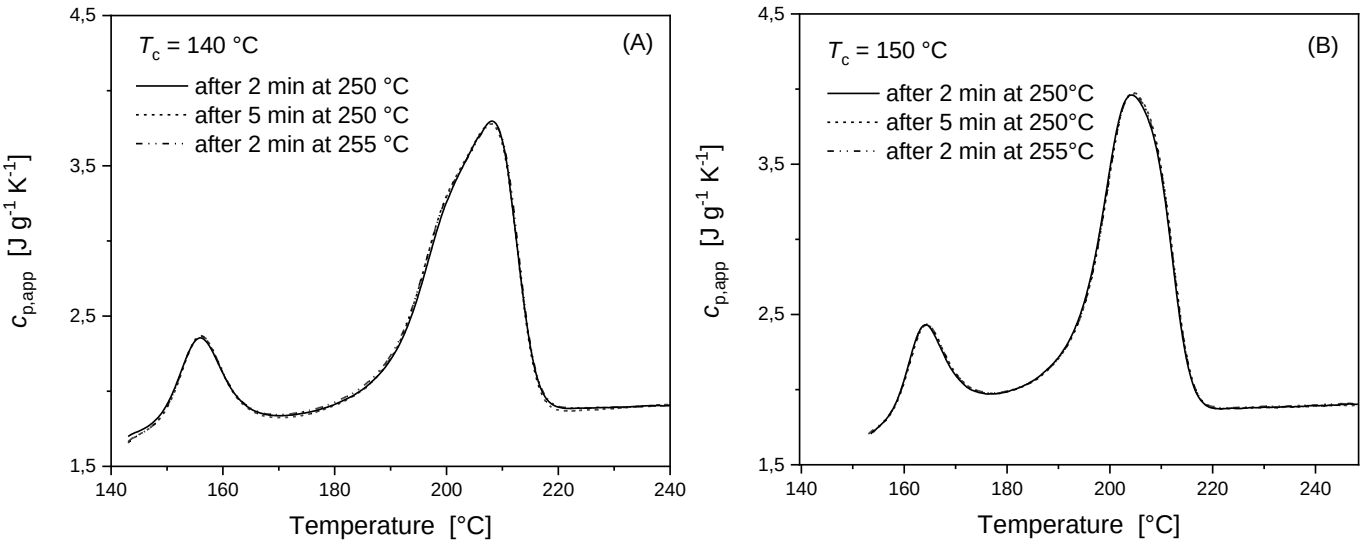

Fig. S2. Apparent specific heat capacity ($c_{p,app}$) curves at 10 K min^{-1} after the initial thermal treatments indicated in the legends and isothermal crystallization at different T_cs: (A) 120 min at T_c = 140 °C, (B) 90 min at T_c = 150 °C.

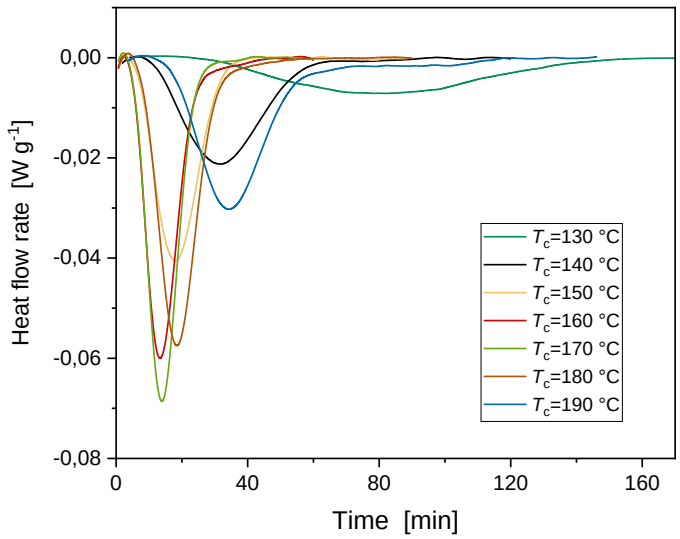

Fig. S3. Heat flow rate signal during isothermal crystallization of PEF at the indicated T_cs.

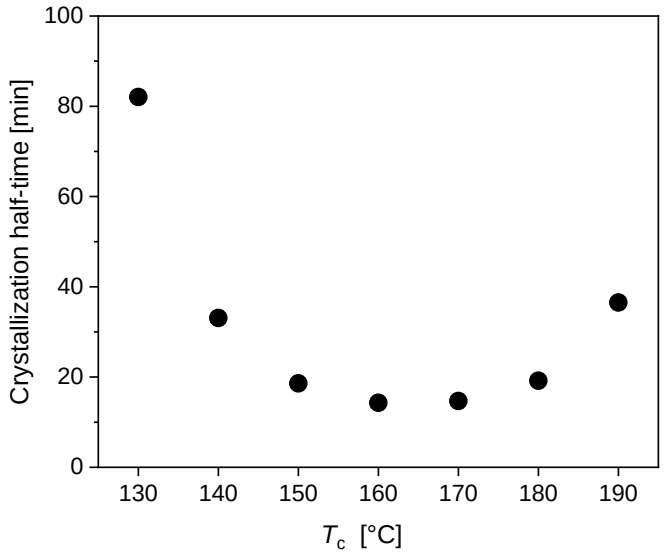

Fig. S4. Crystallization half-time as a function of the crystallization temperature.

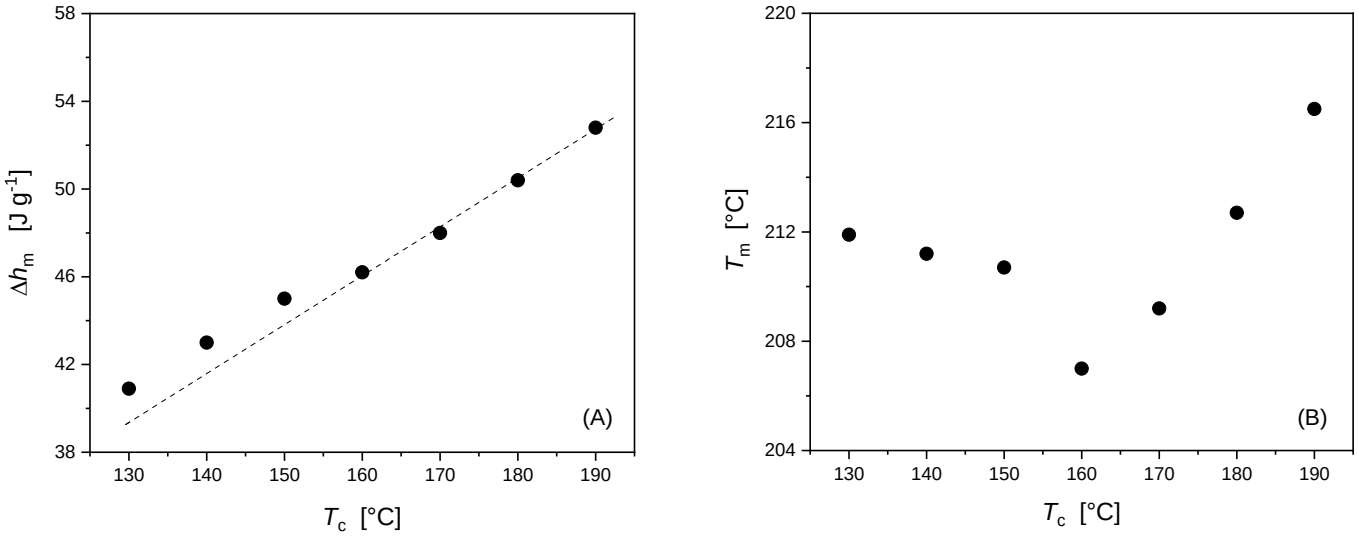

Fig. S5. (A) Enthalpy of melting (Δh_m) measured at 10 K min^{-1} as a function of T_c. The dashed line is a guide to the eye. (B) Peak temperature of the highest melting peak (T_m) measured at 10 K min^{-1} as a function of T_c.

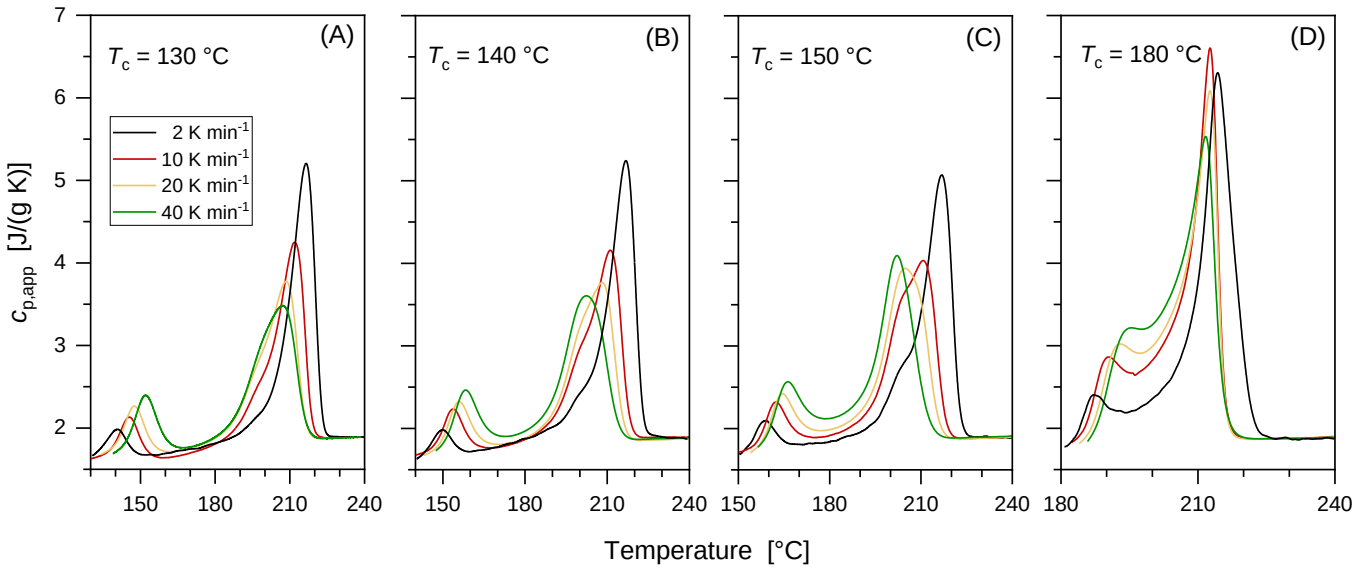

Fig. S6. Apparent specific heat capacity ($c_{p,app}$) curves at different heating rates after isothermal crystallization at various T_cs.

The occurring of intense melting/recrystallization/remelting process upon heating after crystallization at T_c =130, 140 and 150 °C is attested in Figure S6 by the relative position and approximate area of the different peaks. The area of the first peak increases and the final melting endotherm shifts to lower temperatures with increasing the heating rate, due to the lower time available for recrystallization. Concerning the peak located at the lowest temperatures, previous studies on PEF ad PET demonstrated that it can be connected to the fusion of imperfect secondary crystals, which melt before the more perfect primary lamellae due to their lower stability [1-3]. Fusion of the original or lightly perfected lamellar crystals, grown at T_c by primary crystallization, is commonly associated to the second peak [1-3]. The large final endotherm after crystallization at T_c = 130, 140 and 150 °C is clearly due to the overlapping of two peaks, because it changes systematically with increasing the heating rate, with the peak at the highest temperatures, or third peak, originating from the fusion of recrystallized crystals. With increasing the perfection of the original crystals, i.e. by increasing T_c, recrystallization occurs at a lower extent and the ratio between the area of the second and

the third peaks increases. After crystallization at T_c = 180 °C, the melting behavior is less dependent on the heating rate: the final endotherm appears single, which proves that it is linkable to the fusion of the original or only lightly perfected α-crystals grown at T_c = 180 °C, which do not undergo recrystallization into a different crystalline population upon heating.

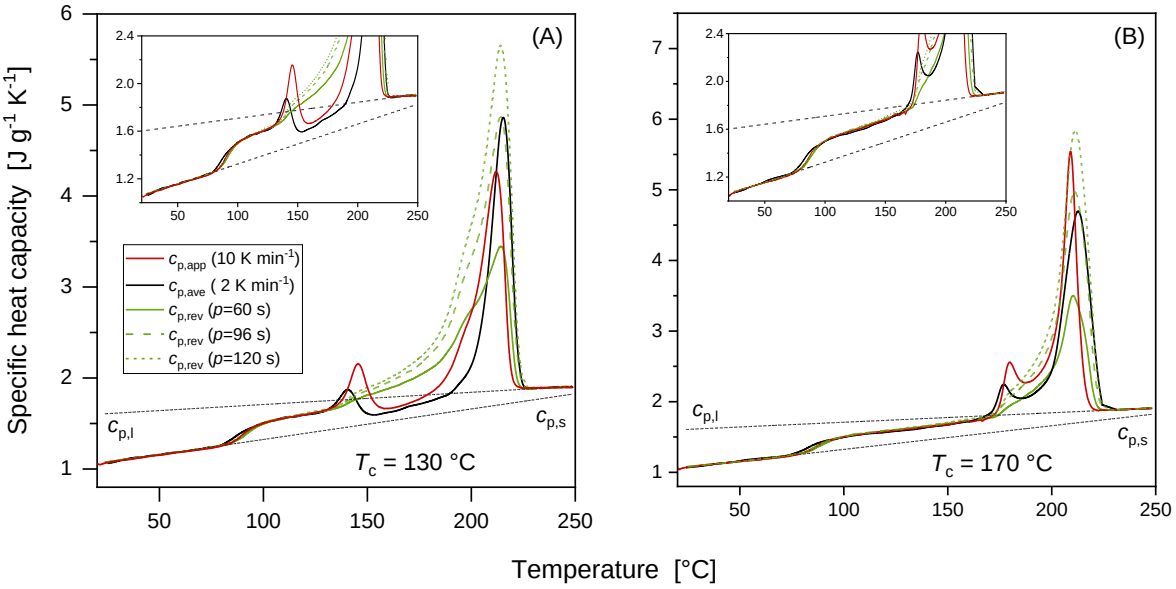

Fig. S7. Specific heat capacities of PEF after crystallization at (A) T_c = 130 °C and (B) T_c = 170 °C as a function of temperature: apparent specific heat capacity ($c_{p,app}$) at 10 K min^{-1}, average specific heat capacity ($c_{p,ave}$) and reversing specific heat capacity ($c_{p,rev}$) at 2 K min^{-1} (p = 60, 96 and 120 s, A_T = 1.0 K). The dotted black lines are the thermodynamic solid and liquid specific heat capacities ($c_{p,s}$ and $c_{p,l}$) of PEF. The insets are enlargements.

C. Numerical correlation between the increased crystallinity upon heating measured by XRD and the Δh_m values determined after isothermal crystallization by DSC

An increase in crystallinity of about 0.07 was measured by XRD for the PEF sample crystallized at T_c =140 °C, after heating up to 190 °C (see text referring to Figure 4 in the paper). If this additional crystallization occurs at about 160 °C, an enthalpy of crystallization of about 9 J g^{-1} can be estimated, by assuming for the temperature dependence of $\Delta h_m°$ the equation reported in the paper for the α-crystals. If these additional crystals melt at about 210 °C, the corresponding enthalpy of melting would be about 10 J g^{-1}. The difference between the enthalpy of melting and the enthalpy of crystallization would be about 1 J g^{-1}, in perfect agreement with the distance between the measured Δh_m values for $T_c \leq 150$ °C and the extrapolated Δh_m line (dashed line in Figure S5(A)).

As declared above, for this estimation the $\Delta h_m°(T)$ of the α-crystals was applied. However, as $\Delta c_p(T)$ was found independent of the crystalline form [see Figure 1 in the paper], the linear and quadratic coefficients of the $\Delta h_m°(T)$ expression are identical for the α'- and α-phases [see Equation (2) in the paper]. This means that $\Delta h_m°$ for the two crystal forms would differ only in the constant term, whereas the temperature dependence is the same, thus confirming the substantial reliability of the above estimation.

References

[1] G. Stoclet, G. Gobius du Sart, B. Yeniad, S. de Vos, J.M. Lefebvre, Isothermal crystallization and structural characterization of poly(ethylene-2,5-furanoate), Polymer 72 (2015) 165−176, https://doi.org/10.1016/j.polymer.2015.07.014.

[2] G. Stoclet, A. Arias, B. Yeniad, S. de Vos, Relationships Between Crystalline Structure and the Thermal Behavior of Poly(ethylene 2,5-furandicarboxylate): An In Situ Simultaneous SAXS-WAXS Study, Polym. Eng. Sci. 59 (2019) 1667−1677, https://doi.org/10.1002/pen.25165.

[3] Y. Kong, J.N. Hay, Multiple melting behavior of poly(ethylene terephthalate), Polymer 44 (2003) 623−633, https://doi.org/10.1016/S0032-3861(02)00814-5.